

RESEARCH ARTICLE SUMMARY

COSMOCHEMISTRY

Macromolecular organic matter in samples of the asteroid (162173) Ryugu

Hikaru Yabuta* *et al.*

INTRODUCTION: Organic compounds in asteroids and comets contain information about the early history of the Solar System. They could also have delivered organic material to early Earth. The Hayabusa2 spacecraft visited the carbonaceous asteroid Ryugu and collected samples of its surface materials, which were brought to Earth in December 2020.

RATIONALE: We investigated the macromolecular organic matter in the Ryugu samples, measuring its elemental, isotopic, and functional group compositions along with its small-scale structures and morphologies. Analytical methods used included spectro-microscopies, electron microscopy, and isotopic microscopy. We examined intact Ryugu grains and insoluble carbonaceous residues isolated by acid treatment of the Ryugu samples.

RESULTS: Organic matter is abundant in the Ryugu grains, distributed as submicrometer-sized organic grains and as organic matter dispersed in matrix. The Ryugu organic matter consists of aromatic carbons, aliphatic carbons, ketones, and carboxyls. The functional group

compositions are consistent with those of insoluble organic matter (IOM) from primitive carbonaceous CI (Ivuna-type) and CM (Mighei-type) chondritic meteorites. Those meteorites experienced aqueous alteration (reactions with liquid water) on their parent bodies, which implies that the Ryugu organic matter was also modified by aqueous alteration on the asteroid parent body.

The functional group distributions of the Ryugu organic matter vary on submicrometer scales in ways that relate to the morphologies: nanoparticulate and/or nanoglobular regions are aromatic-rich, whereas organic matter associated with Mg-rich phyllosilicate matrix and carbonates is IOM-like or occurs as diffuse carbon. The observed macromolecular diversity provides further evidence that the organics were modified by aqueous alteration on Ryugu's parent body. The diffuse carbon is similar to clay-bound organic matter that occurs in CI chondrites and the ungrouped C2-type meteorite Tagish Lake. No graphite-like material was found, which indicates that the Ryugu organic matter was not subjected to heating events on the parent body.

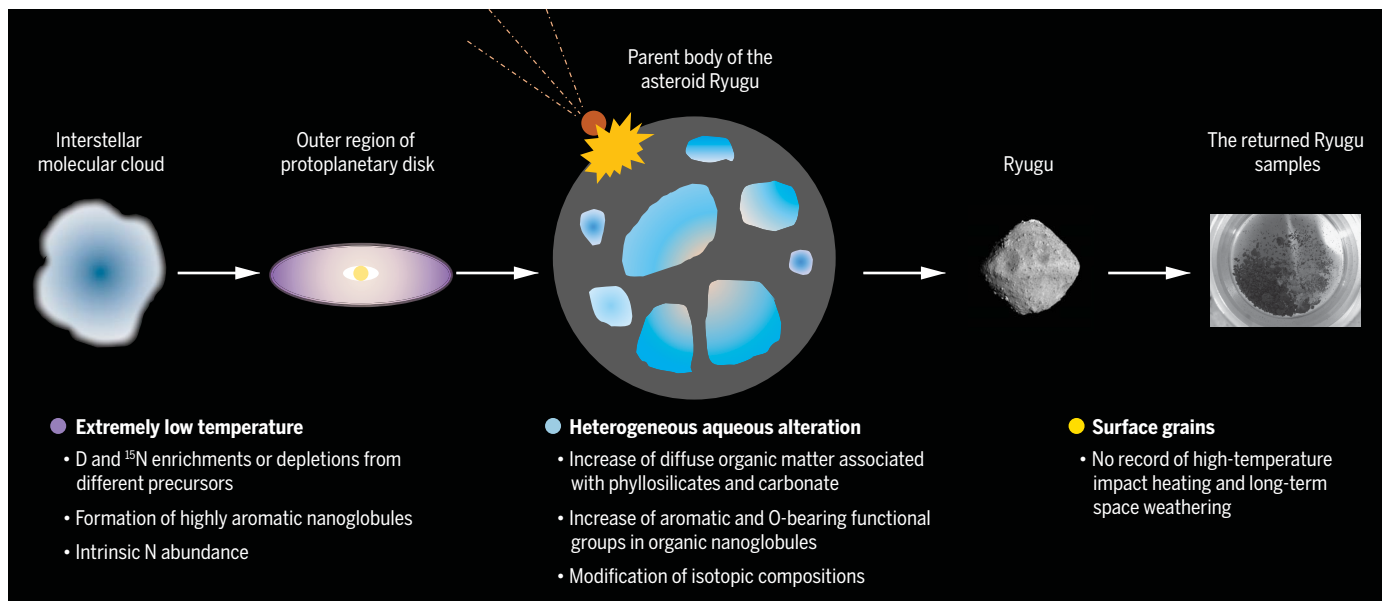
The bulk hydrogen and nitrogen isotopic ratios of the Ryugu grains are between the bulk values of CI chondrites and the IOM in CI chondrites. Some carbonaceous grains showed extreme deuterium (D) and/or nitrogen-15 (^{15}N) enrichments or depletions. These indicate an origin in the interstellar medium or presolar nebula. The bulk hydrogen isotopic ratios of insoluble carbonaceous residues from the Ryugu samples are lower than those in CI and CM chondrites. The range of D enrichments are consistent with the ranges of CI, CM, and Tagish Lake chondrites. The nitrogen isotopic ratios of the IOM from Ryugu samples were close to those in CI chondrites.

CONCLUSION: The organic matter in Ryugu probably consists of primordial materials that formed during (or before) the early stages of the Solar System's formation, which were later modified by heterogeneous aqueous alteration on Ryugu's parent body asteroid. Although the surface of Ryugu is exposed to solar wind, impacts, and heating by sunlight, the macromolecular organics in the surface grains of Ryugu are similar in their chemical, isotopic, and morphological compositions to those seen in primitive carbonaceous chondrites. The properties of Ryugu's organic matter could explain the low albedo of the asteroid's surface. ■

The complete list of authors and their affiliations is available in the full article online.

*Corresponding author. Email: hyabuta@hiroshima-u.ac.jp
Cite this article as H. Yabuta *et al.*, *Science* **379**, eabn9057 (2023). DOI: 10.1126/science.abn9057

S READ THE FULL ARTICLE AT
<https://doi.org/10.1126/science.abn9057>



Chemical evolution of macromolecular organic matter in samples of asteroid Ryugu. Organic matter formed in the interstellar medium or in the outer region of the protoplanetary disk that formed the Solar System. It was then incorporated into a planetesimal—Ryugu's parent body—where it experienced varying degrees of reactions with liquid water. An impact ejected material from the parent body, which reassembled to form Ryugu. Samples were brought to Earth by Hayabusa2.

RESEARCH ARTICLE

COSMOCHEMISTRY

Macromolecular organic matter in samples of the asteroid (162173) Ryugu

Hikaru Yabuta^{1*†}, George D. Cody², Cécile Engrand³, Yoko Kebukawa⁴, Bradley De Gregorio⁵, Lydie Bonal⁶, Laurent Remusat⁶, Rhonda Stroud^{5‡}, Eric Quirico⁶, Larry Nittler^{2§}, Minako Hashiguchi⁸, Mutsumi Komatsu^{9,10}, Taiga Okumura¹¹, Jérémie Mathurin¹², Emmanuel Dartois¹³, Jean Duprat⁷, Yoshio Takahashi^{11,14}, Yasuo Takeichi¹⁴, David Kilcoyne^{15¶}, Shohei Yamashita¹⁴, Alexandre Dazzi¹², Ariane Deniset-Besseau¹², Scott Sandford¹⁶, Zita Martins¹⁷, Yusuke Tamenori¹⁸, Takuji Ohigashi¹⁹, Hiroki Suga¹⁸, Daisuke Wakabayashi¹⁴, Maximilien Verdier-Paoletti⁷, Smail Mostefaoui⁷, Gilles Montagnac²⁰, Jens Barosch², Kanami Kamide¹, Miho Shigenaka¹, Laure Bejach³, Megumi Matsumoto²¹, Yuma Enokido²¹, Takaaki Noguchi²², Hisayoshi Yurimoto²³, Tomoki Nakamura²¹, Ryuji Okazaki²⁴, Hiroshi Naraoka²⁴, Kanako Sakamoto²⁵, Harold C. Connolly Jr.²⁶, Dante S. Lauretta²⁷, Masanao Abe^{25,28}, Tatsuaki Okada^{25,29}, Toru Yada²⁵, Masahiro Nishimura²⁵, Kasumi Yogata²⁵, Aiko Nakato²⁵, Miwa Yoshitake²⁵, Ayako Iwamae³⁰, Shizuho Furuya¹¹, Kentaro Hatakeda³⁰, Akiyo Miyazaki²⁵, Hiromichi Soejima³⁰, Yuya Hitomi³⁰, Kazuya Kumagai³⁰, Tomohiro Usui²⁵, Tasuku Hayashi²⁵, Daiki Yamamoto²⁵, Ryota Fukai²⁵, Seiji Sugita^{11,31}, Kohei Kitazato³², Naru Hirata³², Rie Honda³³, Tomokatsu Morota¹¹, Eri Tatsumi³⁴, Naoya Sakatani³⁵, Noriyuki Namiki^{28,36}, Koji Matsumoto^{28,36}, Rina Noguchi³⁷, Koji Wada³¹, Hiroki Senshu³¹, Kazunori Ogawa³⁸, Yasuhiro Yokota²⁵, Yoshiaki Ishihara³⁸, Yuri Shimaki²⁵, Manabu Yamada³¹, Chikatashi Honda³², Tatsuhiro Michikami³⁹, Moe Matsuoka⁴⁰, Naoyuki Hirata⁴¹, Masahiko Arakawa⁴¹, Chisato Okamoto^{41¶}, Masateru Ishiguro⁴², Ralf Jaumann⁴³, Jean-Pierre Bibring⁴⁴, Matthias Grott⁴⁵, Stefan Schröder⁴⁶, Katharina Otto^{1,45}, Cedric Pilorget^{44,47}, Nicole Schmitz⁴⁵, Jens Biele⁴⁸, Tra-Mi Ho⁴⁹, Aurélie Moussi-Soffys⁵⁰, Akira Miura²⁵, Hirotomo Noda^{28,36}, Tetsuya Yamada²⁵, Keisuke Yoshihara²⁵, Kosuke Kawahara²⁵, Hitoshi Ikeda²⁵, Yukio Yamamoto²⁵, Kei Shirai⁴¹, Shota Kikuchi^{31,36}, Naoko Ogawa²⁵, Hiroshi Takeuchi^{25,28}, Go Ono⁵¹, Yuya Mimasu²⁵, Kent Yoshikawa⁵¹, Yuto Takei²⁵, Atsushi Fujii²⁵, Yu-ichi Iijima^{25¶}, Satoru Nakazawa²⁵, Satoshi Hosoda²⁵, Takahiro Iwata^{25,28}, Masahiko Hayakawa²⁵, Hirotaka Sawada³⁸, Hajime Yano^{25,28}, Ryudo Tsukizaki²⁵, Masanobu Ozaki^{25,28}, Fuyuto Terui⁵², Satoshi Tanaka^{25,28}, Masaki Fujimoto²⁵, Makoto Yoshikawa^{25,28}, Takanao Saiki²⁵, Shogo Tachibana^{11,25}, Sei-ichiro Watanabe⁸, Yuichi Tsuda²⁵

Samples of the carbonaceous asteroid (162173) Ryugu were collected and brought to Earth by the Hayabusa2 spacecraft. We investigated the macromolecular organic matter in Ryugu samples and found that it contains aromatic and aliphatic carbon, ketone, and carboxyl functional groups. The spectroscopic features of the organic matter are consistent with those in chemically primitive carbonaceous chondrite meteorites that experienced parent-body aqueous alteration (reactions with liquid water). The morphology of the organic carbon includes nanoglobules and diffuse carbon associated with phyllosilicate and carbonate minerals. Deuterium and/or nitrogen-15 enrichments indicate that the organic matter formed in a cold molecular cloud or the presolar nebula. The diversity of the organic matter indicates variable levels of aqueous alteration on Ryugu's parent body.

Organic compounds in asteroids and comets were produced and modified within the presolar molecular cloud, the protoplanetary disk, during the formation of planetesimals in the early Solar System and their subsequent evolution. Delivery of extraterrestrial organic compounds might have contributed to the habitability of terrestrial planets, including Earth. Analysis of pristine samples collected from primitive small bodies (asteroids and comets) could provide information on how organic compounds were formed and modified in space and which organic compounds were supplied to early Earth. Macromolecular organic matter, a dark, complex acid-insoluble organic matter (IOM), accounts for most carbon in primitive carbonaceous chondrite meteorites.

The Hayabusa2 asteroid sample return mission visited the carbonaceous (C-type) asteroid (162173) Ryugu. The mission goals included investigating the origin and evolution of organic compounds in the early Solar System (1). Remote sensing and lander observations showed that Ryugu is a dark, rubble-pile asteroid that contains hydrated minerals on its surface (2–4) and indicated a relationship between C-type asteroids and carbonaceous chondrites (3, 4). The average albedo of Ryugu is consistent with the thermally metamorphosed subgroups of the CI1 and CM2 meteorites (3, 4). CI1 meteorites are Ivuna-type carbonaceous chondrites of petrologic type 1 (extensively altered by aqueous fluids on the parent asteroid), and CM2 meteorites are Mighei-type carbonaceous chondrites of petrologic type 2

(moderately aqueously altered). Spectral and thermal inertia variations indicated that Ryugu consists of boulders that experienced different degrees of thermal and space weathering processes (5–7), derived from a much larger parent body and potentially additional materials from different asteroids (8).

The Hayabusa2 spacecraft collected the surface material from two touchdown sites on Ryugu and returned them to Earth on 6 December 2020. The Ryugu samples exhibit near-infrared absorption features as a result of OH and carbonate and/or organic C-H bonds, at 2.7 and 3.4 μm respectively (9, 10), which indicates that the Ryugu samples are similar to CI carbonaceous chondrites (9).

We sought to determine the distributions and chemical characteristics of macromolecular organic matter in the Ryugu samples. We therefore measured the elemental, isotopic, and functional group compositions, structures, and textures of organic macromolecules from the Ryugu samples. The analytical procedures included micro-Fourier transform infrared (FTIR) spectroscopy, micro-Raman spectroscopy, synchrotron-based scanning transmission x-ray microscopy (STXM), x-ray absorption near-edge structure (XANES), scanning transmission electron microscopy (STEM) coupled with electron energy-loss spectroscopy (EELS) and energy-dispersive x-ray spectroscopy (EDS), atomic force microscope-based infrared (AFM-IR) spectroscopy, and nanometer-scale secondary ion mass spectrometry (NanoSIMS) (11). The analytical workflow (fig. S1) was designed to optimize the use of these complementary techniques.

The samples we used were selected aggregates stored in collection chamber A (from the first touchdown) and collection chamber C (from the second touchdown) of the spacecraft sample catcher (12) (table S1). We studied (i) intact grains (taken from aggregates designated A0108 and C0109), ranging from 200 to 900 nm in size per particle, and (ii) insoluble carbonaceous residues (fig. S2) isolated by acid treatment of Ryugu aggregates (designated A0106 and C0107). Each of these samples was split into several subsamples for analysis with different techniques (table S1).

Structural properties of macromolecular organic matter

To characterize the macromolecular structures of organic matter in Ryugu, we applied micro-Raman spectroscopy. Two peaks, identified as the D-band ($\sim 1350\text{ cm}^{-1}$) and G-band ($\sim 1580\text{ cm}^{-1}$) of polyaromatic molecular structures (13), are present in the Raman spectra of A0108 and C0109 (Fig. 1A and fig. S3A). The spectral features are broad, indicating lattice disorder in the organic macromolecules, and are superimposed on a fluorescence background. The numerical values of the derived

spectral parameters of the D- and G-bands, such as their full widths at half maximum (FWHM_D and FWHM_G, respectively), peak positions (ω_D and ω_G), and intensity ratio (I_D/I_G), are similar for all grains examined from the two aggregates (Fig. 1, B to D, and fig. S3, B to D).

The macromolecular structures of organic matter in meteorites reflect the thermal histories of the meteorite parent bodies (13–16). To evaluate the thermal history of Ryugu, we compared the Raman parameters measured from the Ryugu samples with those measured from meteorites (Fig. 1, B to D, and fig. S3, B to D). The closest matches to Ryugu are the primitive CI1 and CM2 carbonaceous chondrites. The Ryugu samples are distinct from carbonaceous chondrites of petrologic type 3 (thermally metamorphosed) (Fig. 1B) and from the thermally metamorphosed subgroup of CM2, such as the Jbilet Winselwan meteorite (Fig. 1, C and D), and other ungrouped carbonaceous chondrites of petrologic type 2 (C2), such as the Wisconsin Range (WIS) 91600 and Peora Escarpment (PCA) 02012 meteorites (Fig. 1, C and D). This indicates that the Ryugu samples A0108 and C0109 did not experience long-duration radiogenic thermal metamorphism on their parent bodies, as petrologic type 3 chondrites did (17), or impact-induced, short-duration heating, as experienced by some petrologic type 2 chondrites (18).

Functional group compositions

We used micro-FTIR spectroscopy to characterize the organic molecules and minerals. The FTIR spectra of the Ryugu grains show bands

due to organic aliphatic C-H stretching (3000 to 2800 cm^{-1} , 3.33 to 3.57 μm), aromatic C=C stretching ($\sim 1600 \text{ cm}^{-1}$, $\sim 6.25 \mu\text{m}$), and carbonyl C=O stretching modes ($\sim 1700 \text{ cm}^{-1}$, $\sim 5.88 \mu\text{m}$), as well as bands due to mineral Si-O stretching ($\sim 1000 \text{ cm}^{-1}$, $\sim 10.00 \mu\text{m}$), structural OH stretching of phyllosilicates ($\sim 3680 \text{ cm}^{-1}$, $\sim 2.72 \mu\text{m}$), and the ν_3 stretching mode of carbonates ($\sim 1435 \text{ cm}^{-1}$, $\sim 6.97 \mu\text{m}$) (Fig. 2A). The spectra also contain bands from interlayer water, of varying intensities, contributing at $\sim 3300 \text{ cm}^{-1}$ ($\sim 3.03 \mu\text{m}$; stretching) and 1640 cm^{-1} (6.10 μm ; bending). Part of this water is intrinsic to the Ryugu grains, and part can be attributed to water adsorbed on the grains under atmospheric conditions.

These absorption bands are commonly observed in unheated, aqueously altered carbonaceous chondrites (19, 20), whereas organic features are weaker in thermally metamorphosed CM chondrites, such as the Jbilet Winselwan meteorite (Fig. 2A). The spectral shape of the OH band in the Ryugu samples is characteristic of Mg-rich phyllosilicates, which have been observed in CI chondrites as saponite and serpentine (21, 22). There were large spectral heterogeneities among the Ryugu grains, but there is no obvious difference in the spectral variations observed between samples from chambers A and C. Compared with CI chondrites, the sulfate S=O stretching band (~ 1100 to 1200 cm^{-1} , ~ 9.09 to $8.33 \mu\text{m}$) is absent from the spectra of Ryugu samples. The absence of sulfates is consistent with other elemental and mineralogical measurements of Ryugu samples (23, 24). Sulfate can be produced by oxidation of sulfides during terrestrial weathering of the meteorites (25), so the

lack of sulfate indicates that the Ryugu samples are pristine (23).

The shapes of the FTIR spectra of the grains are consistent with the reflectance spectra of Ryugu's surface acquired by the Hayabusa2 spacecraft (4). The OH band and aliphatic C-H band features in our absorption spectra are similar to reflectance spectra of other Ryugu samples (9), but we find lower intensities of aliphatic C-H peaks.

The FTIR spectra of insoluble carbonaceous residues obtained from our Ryugu samples show similar functional groups to those of the intact Ryugu grains (Fig. 2B). The aliphatic C-H stretching band (3000 to 2800 cm^{-1} , 3.33 to 3.57 μm) from the carbonaceous residue from Ryugu is more intense than those of IOM from meteorites (26, 27). The peak intensity ratios of CH_2 to CH_3 ($I_{\text{CH}_2}/I_{\text{CH}_3}$) of the Ryugu residues are 1.9, whereas those of IOMs in Murchison and Ivuna meteorites are 1.2 and 1.3, respectively. Because $I_{\text{CH}_2}/I_{\text{CH}_3}$ ratios are proportional to the molar ratios of CH_2 to CH_3 (CH_2/CH_3), we infer the CH_2/CH_3 ratios of the residue, which are higher than those of meteoritic IOMs. This could indicate that Ryugu's organic matter contains longer aliphatic chains, or aliphatic chains with a higher degree of cross-linking. The Ryugu carbonaceous residue also exhibits an absorption band of C=O ($\sim 1670 \text{ cm}^{-1}$, $\sim 5.99 \mu\text{m}$), which is not seen in meteoritic IOMs. We assign this C=O band to unsaturated ketones, aldehydes, or amides.

Chemical and morphological variations Macromolecular diversity

We used synchrotron-based STXM, with spatial resolution of 30 to 50 nm, to produce

¹Department of Earth and Planetary Systems Science, Hiroshima University, Hiroshima 739-8526, Japan. ²Earth and Planets Laboratory, Carnegie Institution for Science, Washington, DC 20015, USA. ³Laboratoire de Physique des 2 Infinis Irène Joliot-Curie, Université Paris-Saclay, Centre National de la Recherche Scientifique, 91405 Orsay, France. ⁴Faculty of Engineering, Yokohama National University, Yokohama 240-8501, Japan. ⁵Materials Science and Technology Division, US Naval Research Laboratory, Washington, DC 20375, USA. ⁶Institut de Planétologie et d'Astrophysique, Université Grenoble Alpes, 38000 Grenoble, France. ⁷Institut de Minéralogie, Physique des Matériaux et Cosmochimie, Muséum National d'Histoire Naturelle, Centre National de la Recherche Scientifique, Sorbonne Université, 75231 Paris, France. ⁸Graduate School of Environmental Studies, Nagoya University, Nagoya 464-8601, Japan. ⁹Center for University-Wide Education, Saitama Prefectural University, Saitama 343-8540, Japan. ¹⁰Department of Earth Sciences, Waseda University, Tokyo 169-8050, Japan. ¹¹Department of Earth and Planetary Science, The University of Tokyo, Tokyo 113-0033, Japan. ¹²Institut Chimie Physique, Université Paris-Saclay, Centre National de la Recherche Scientifique, 91405 Orsay, France. ¹³Institut des Sciences Moléculaires d'Orsay, Université Paris-Saclay, Centre National de la Recherche Scientifique, 91405 Orsay, France. ¹⁴Institute of Materials Structure Science, High Energy Accelerator Research Organization, Tsukuba 305-0801, Japan. ¹⁵Advanced Light Source, Lawrence Berkeley National Laboratory, Berkeley, CA 94720, USA. ¹⁶NASA Ames Research Center, Moffett Field, CA 94035, USA. ¹⁷Centro de Química Estrutural, Institute of Molecular Sciences and Department of Chemical Engineering, Instituto Superior Técnico, Universidade de Lisboa, Lisboa 1049-001, Portugal. ¹⁸Japan Synchrotron Radiation Research Institute, Hyogo 679-5198, Japan. ¹⁹Institute for Molecular Science, UVSOR Synchrotron Facility, Okazaki 444-8585, Japan. ²⁰École normale supérieure de Lyon, University Lyon 1, 69342 Lyon, France. ²¹Department of Earth Science, Tohoku University, Sendai 980-8578, Japan. ²²Department of Earth and Planetary Sciences, Kyoto University, Kyoto 606-8502, Japan. ²³Department of Earth and Planetary Sciences, Hokkaido University, Sapporo 060-0810, Japan. ²⁴Department of Earth and Planetary Sciences, Kyushu University, Fukuoka 819-0395, Japan. ²⁵Institute of Space and Astronautical Science, Japan Aerospace Exploration Agency (JAXA), Sagami-hara 252-5210, Japan. ²⁶Department of Geology, School of Earth and Environment, Rowan University, Glassboro, NJ 08028, USA. ²⁷Lunar and Planetary Laboratory, University of Arizona, Tucson, AZ 85721, USA. ²⁸School of Physical Sciences, The Graduate University for Advanced Studies, Hayama 240-0193, Japan. ²⁹Department of Chemistry, The University of Tokyo, Tokyo 113-0033, Japan. ³⁰Marine Works Japan Ltd., Yokosuka 237-0063, Japan. ³¹Planetary Exploration Research Center, Chiba Institute of Technology, Narashino 275-0016, Japan. ³²Aizu Research Cluster for Space Science, University of Aizu, Aizu-Wakamatsu 965-8580, Japan. ³³Center of Data Science, Ehime University, Matsuyama 790-8577, Japan. ³⁴Instituto de Astrofísica de Canarias, University of La Laguna, Tenerife E-38205, Spain. ³⁵Department of Physics, Rikkyo University, Tokyo 171-8501, Japan. ³⁶Research of Interior Structure and Evolution of Solar System Bodies, National Astronomical Observatory of Japan, Mitaka 181-8588, Japan. ³⁷Faculty of Science, Niigata University, Niigata 950-2181, Japan. ³⁸JAXA Space Exploration Center, JAXA, Sagami-hara 252-5210, Japan. ³⁹Faculty of Engineering, Kindai University, Higashi-Hiroshima 739-2116, Japan. ⁴⁰Geological Survey of Japan, National Institute of Advanced Industrial Science and Technology, Tsukuba 305-8567, Japan. ⁴¹Department of Planetology, Kobe University, Kobe 657-8501, Japan. ⁴²Department of Physics and Astronomy, Seoul National University, Seoul 08826, Republic of Korea. ⁴³Freie Universität Berlin, Institute of Geological Sciences, Planetary Sciences and Remote Sensing, Berlin 12249, Germany. ⁴⁴Institut d'Astrophysique Spatiale, Université Paris-Saclay, Centre National de la Recherche Scientifique, 91405 Orsay, France. ⁴⁵Institute of Planetary Research, German Aerospace Center, Berlin 12489, Germany. ⁴⁶Department of Computer Science, Electrical and Space Engineering, Luleå University of Technology, 98128 Kiruna, Sweden. ⁴⁷Institut Universitaire de France, 75005 Paris, France. ⁴⁸Microgravity User Support Centre, German Aerospace Center, Cologne 53147, Germany. ⁴⁹Institute of Space Systems, German Aerospace Center, Bremen 28359, Germany. ⁵⁰Centre National d'Études Spatiales, 31401 Toulouse, France. ⁵¹Research and Development Directorate, JAXA, Sagami-hara 252-5210, Japan. ⁵²Department of Mechanical Engineering, Kanagawa Institute of Technology, Atsugi 243-0292, Japan.

*Corresponding author. Email: hyabuta@hiroshima-u.ac.jp

†Present address: International Institute for Sustainability with Knotted Chiral Meta Matter, Hiroshima University, Hiroshima 739-8526, Japan.

‡Present address: Buseck Center for Meteorite Studies, Arizona State University, Tempe, AZ 85827, USA.

§Present address: School of Earth and Space Exploration, Arizona State University, Tempe, AZ 85827, USA. ¶Deceased.

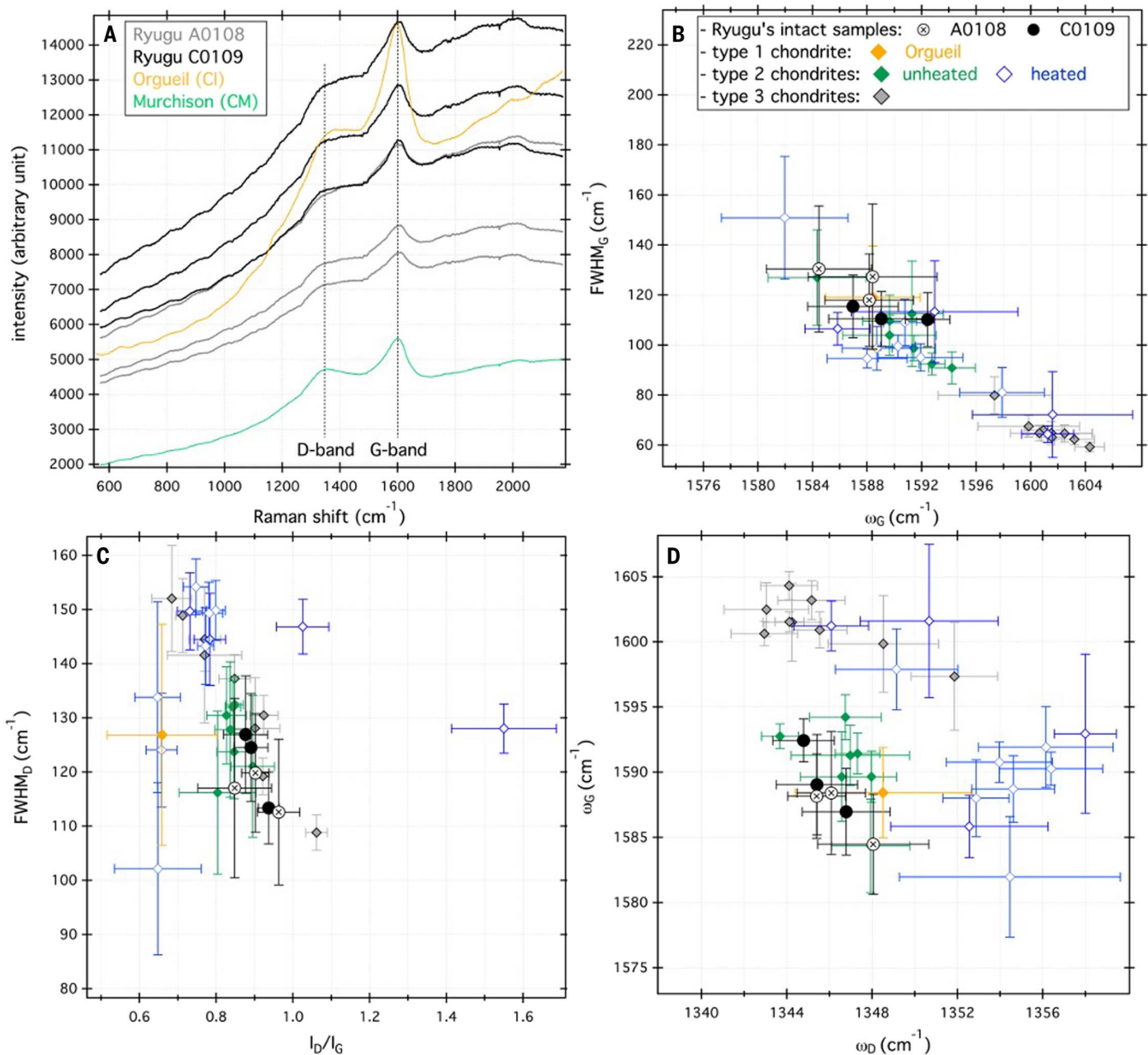


Fig. 1. Raman spectra and spectral parameters: Comparison between Ryugu samples and chondrites. (A) Average Raman spectra of Ryugu grains from chamber A (samples A0108-6, -10, and -18) (in gray) and chamber C (samples C0109-5, -9, and -12) (in black) compared with the meteorites Murchison (CM; green) and Orgueil (CI; yellow). All spectra were acquired in the same analytical conditions (11). (B to D) Average spectral parameters (error bars show standard deviations) determined from the Raman spectra: FWHM_G as a function of ω_G (B);

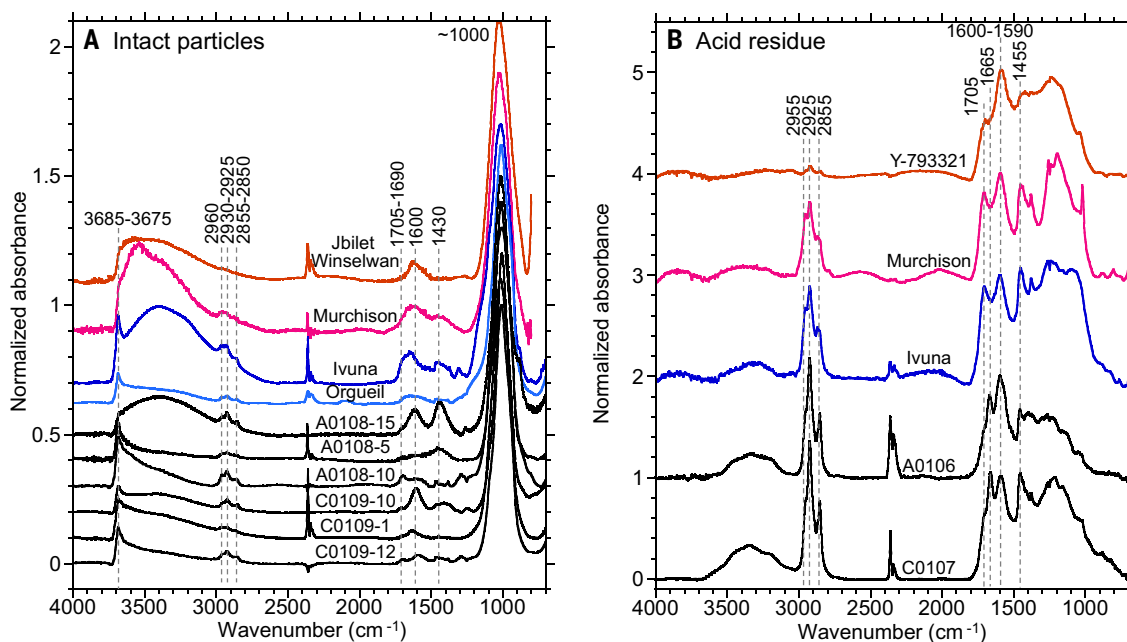
FWHM_D as a function of I_D/I_G (C); and ω_G as a function of ω_D (D). Data are for individual grains from chamber A (open circles) and chamber C (black filled circles) compared with petrologic type 1 (Orgueil; orange diamond), unheated petrologic type 2 chondrites (green filled diamonds), heated petrologic type 2 chondrites (open blue diamonds), and petrologic type 3 chondrites (filled gray diamonds) (11). Petrologic type 2 chondrites were classified (16) as unheated (e.g., Murchison, Nogoya, and Tarda) or heated (e.g., Jbilet Winselwan and WIS 91600).

elemental x-ray maps and XANES spectra. Carbon x-ray maps (Fig. 3, A and B) show discrete grains of organic material with sizes of ~ 200 nm. X-ray absorption by carbon atoms is also present in the phyllosilicate matrix at low levels but nearly ubiquitously (Fig. 3B). Carbon-XANES spectra of the discrete grains show three major peaks, resulting from aro-

matic carbon (C=C, 285 eV), aromatic ketone (C=C-C=O, 286.7 eV), and carboxyl (COOH, 288.5 eV) functional groups (Fig. 3E), which have been observed in primitive extraterrestrial carbonaceous matter, such as carbonaceous chondrites (28, 29) and their extracted IOMs (30), interplanetary dust particles (IDPs) (31), dust particles from Comet Wild 2 (32),

and Antarctic micrometeorites (AMMs) (33). Some spectra of fine-grained matrices in the Ryugu samples contain an additional peak at 290.4 eV, which corresponds to a $1s-\pi^*$ transition of carbonate groups—e.g., in calcite and other carbonate minerals. However, our matrix XANES spectra containing this feature lack extended x-ray absorption fine structure

Fig. 2. Micro-FTIR spectra of Ryugu samples compared with chondrites. (A) Infrared transmission spectra (11) of six Ryugu grains from the aggregates A0108 and C0109 (black), heated CM chondrite (Jbilet Winselwan) (red), unheated CM Murchison (pink), and two CI chondrites Orgueil (light blue) and Ivuna (dark blue). All the spectra were baseline-corrected using spline curves and normalized by the peak height of the band at ~ 1000 cm^{-1} (~ 10.00 μm). Dashed lines indicate identified bands: silicate OH and SiO at 3685 to 3675 cm^{-1} (2.71 to 2.72 μm) and ~ 1000 cm^{-1} (~ 10.00 μm); aliphatic C-H bands at 2960 cm^{-1} (3.38 μm ; CH_3 asymmetric stretching), 2930 to 2925 cm^{-1} (3.41 to 3.42 μm ; CH_2 asymmetric stretching), 2855 to 2850 cm^{-1} (3.50 to 3.51 μm ; CH_3 and CH_2 symmetric stretching), 1460 cm^{-1} (6.85 μm), and 1380 cm^{-1} (7.25 μm ; bending); and other organic features at 1705 to 1690 cm^{-1} (5.87 to 5.92 μm ; C=O) and ~ 1600 cm^{-1} (~ 6.25 μm ; aromatic with some water bending mode contribution). Some spectra show a peak at ~ 1430 cm^{-1} (~ 6.99 μm) due to carbonates. A broad water stretching band at ~ 3400 cm^{-1} (~ 2.94 μm) is observed, which is weaker in samples that were measured at 60°C or higher temperatures. The peaks at 2360 cm^{-1} (4.24 μm) are due to atmospheric CO_2 . The A0108-5 and



A0108-5 and C0109-1 Ryugu grains and the Murchison and Ivuna meteorites were measured at 60°C under N_2 flow. The Jbilet Winselwan meteorite was measured at 80°C under N_2 flow. The A0108-10 and C0109-12 Ryugu grains were measured at 80°C under vacuum. The Orgueil meteorite was measured at 130°C under vacuum. (B) Same as (A), but for insoluble carbonaceous residues from the Ryugu samples (A0106 and C0107) compared with IOM from the heated CM meteorite Y-793321 (16), the CM Murchison (27), and the CI meteorite Ivuna (27). The spectra were the averages of main fractions of A0106 and C0107, respectively, after baseline-correction using spline curves and normalization by the peak height of the aromatic C=C band at ~ 1600 cm^{-1} (~ 6.25 μm).

(EXAFS) features at higher energies (294 to 304 eV), indicating that the carbonate is not in a crystalline structure so is more likely to be molecular carbonate. A similar carbonate feature has previously been reported in clay-bound carbon from extensively hydrated carbonaceous chondrites, Ivuna (CI1), Orgueil (CI1), and Tagish Lake (C2) (34), and in diffuse carbon (organic matter) in the fine-grained matrices of Renazzo (CR2; a Renazzo-type carbonaceous chondrite of petrologic type 2), Murchison (CM2), and Orgueil (28).

We classify the STXM spectra of Ryugu organic matter on the basis of spectral shape similarities into four representative types: (i) highly aromatic ($\sim 25\%$ of individual carbon grains), (ii) aromatic ($\sim 35\%$ of individual grains), (iii) IOM-like ($\sim 40\%$ of individual grains), and (iv) diffuse carbon associated with a molecular carbonate peak (Fig. 3E). Aromatic spectra show higher ratios of aromatic carbon to aromatic ketone compared with IOM-like spectra, whereas highly aromatic spectra show a broader peak for aromatic carbon, indicating increased diversity of aromatic structures. The frequency distributions of these classes were similar for both chamber A and C samples. We find a relationship between the mor-

phology of organic matter and XANES spectral shape, with particulate and nanoglobular regions having more frequent aromatic or highly aromatic XANES spectra, whereas organic matter dispersed in the matrix more commonly has IOM-like or diffuse carbon spectra. These observations indicate that the molecular functional groups present are influenced by aqueous processing on the asteroid parent body. We did not find any evidence of long-duration thermal metamorphism, such as the $1s\text{-}\sigma^*$ exciton (291.6 eV) peak of graphite or other graphitized carbon materials (35).

Similar characteristics are found for the insoluble carbonaceous residues from Ryugu. Average carbon-XANES spectra have IOM-like spectral shapes but with more prominent aromatic C=C, ketone, and carboxyl peaks compared with IOM from Orgueil and Murchison (Fig. 3E). Several hollow and solid organic nanoglobules are apparent in the x-ray absorption images (Fig. 3, C and D), which we confirmed using TEM imaging (Fig. 4, A and B). Their XANES spectra were either IOM-like, aromatic, or highly aromatic (Fig. 3E). The 290.4-eV carbonate feature was not observed in the insoluble carbonaceous residue, perhaps because this organic phase was incor-

porated into phyllosilicate interlayers and so was removed or destroyed during the acid-extraction process.

Nitrogen-XANES spectra (fig. S4A) of the Ryugu intact grains and insoluble residue did not show clear absorption peaks, indicating low abundances of N-rich Ryugu organics. This is consistent with carbonaceous chondrites, where N-rich particles are only occasionally observed (32). Oxygen-XANES spectra (fig. S4B) of Ryugu organic matter often contain a peak at ~ 531.3 eV, corresponding to carbonyl C=O bonds in the ketone and carboxyl functional groups (36). The peak intensity of the carbonyl absorption, relative to the main oxygen $1s\text{-}\sigma^*$ peak in Ryugu, is similar to that of aqueously altered carbonaceous chondrites. We cannot determine whether these carbonyl functional groups are also present in the phyllosilicate-bound diffuse organic matter because its oxygen-XANES spectrum is dominated by the surrounding phyllosilicate.

Nanoscale morphologies

We performed TEM and STEM-EELS-EDS analysis (Fig. 4) on ultrathin sections of particles and carbonaceous residues, including from some of the same sections we analyzed

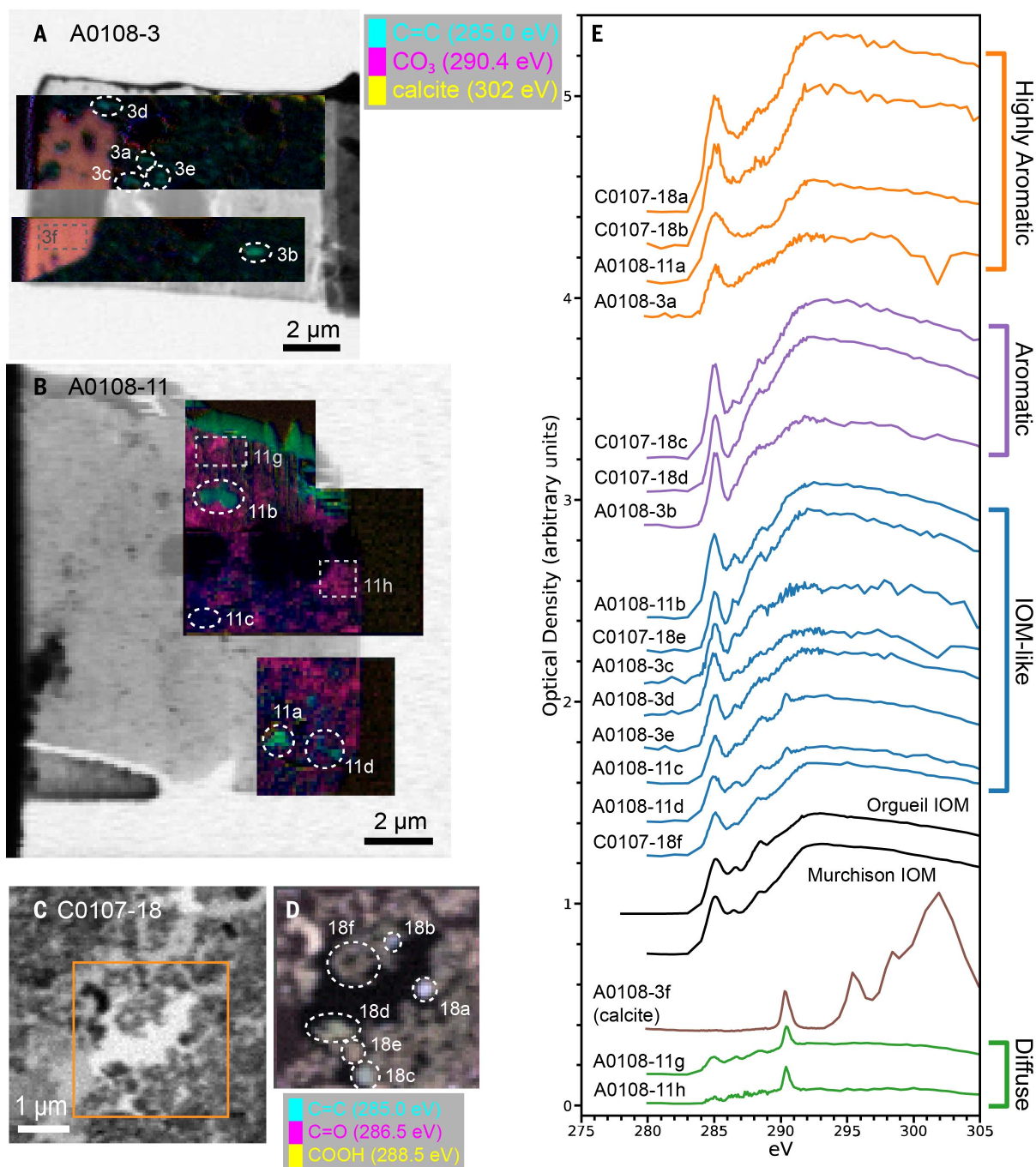


Fig. 3. STXM elemental maps and carbon-XANES spectra of Ryugu samples. (A and B) STXM grayscale images of FIB sections extracted from the Ryugu grains A0108-3, observed at 520 eV (A), and A0108-11, observed at 390 eV (B) (11). In both panels, color overlays on both FIB sections are false-color maps of x-ray absorptions due to aromatic C (cyan), carbonate functional groups (magenta), and calcite minerals (yellow). Dashed circles and boxes indicate regions measured for (E). (C) STXM image at 290 eV of insoluble

carbonaceous residue from Ryugu sample C0107-18. The orange box shows the region in (D). (D) X-ray absorption map of aromatic carbon (cyan), ketones (magenta), and carboxyl (yellow) functional groups. Circled features are solid nanoglobules except for feature 18f, which is a cluster of typical Ryugu IOM. (E) Carbon-XANES spectra for carbonaceous grains and matrix regions identified in (A), (B), and (D). IOM from the meteorites Orgueil and Murchison (black) are shown for comparison (11).

previously with STXM. The two most abundant organic microstructures are nanoglobules (Fig. 4, A and B) and diffuse carbon mixed with phyllosilicates—i.e., clay-bound carbon (Fig. 4, C and E). Other microstructures include dense, irregularly shaped particles (Fig. 4B); diffuse

organic matter trapped in vesicles in carbonate grains (Fig. 4, D and F); and organic matter coatings on sulfide grains. The presence of organic matter associated with Mg-rich phyllosilicates and carbonates, which likely formed through aqueous alteration (24), implies that

much of the organic material was altered by low-temperature, aqueous processing on Ryugu's parent body. However, we also find nanodiamonds associated with amorphous organic carbon, which probably formed in the interstellar medium or the Solar System's protoplanetary

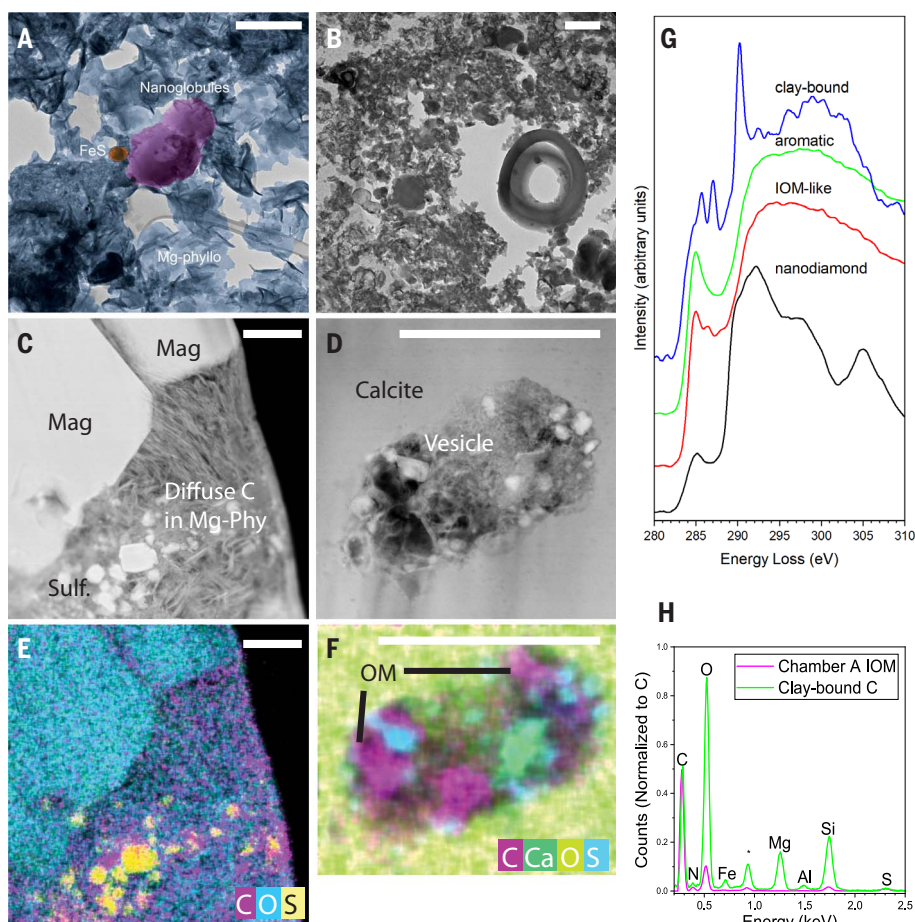


Fig. 4. STEM-EELS-EDS analysis of Ryugu samples. All scale bars are 500 nm. **(A)** False-color bright-field TEM image of the ultrathin section of CO109-11, indicating nanoglobules (magenta), Mg-phyllsilicates (blue), and FeS (orange). **(B)** Bright-field TEM image of insoluble organic residue from a microtome slice of sample CO107, showing hollow and solid nanoglobules and fluffy materials. **(C)** High-angle annular dark field (HAADF) STEM image of a FIB section of A0108-11 (region 11h in Fig. 3B) showing two magnetite grains (labeled Mag) adjacent to carbon-bearing Mg-rich phyllosilicates (Mg-phy) with Fe and Ni sulfide nanoparticles (Sulf). **(D)** HAADF STEM image of a vesicle in the large calcite grain from a FIB section of sample A0108-3 (region 3a in Fig. 3A). **(E)** EDS element map of carbon (magenta), oxygen (cyan), and sulfur (yellow) of the area shown in (C). **(F)** EDS element map of carbon (magenta), calcium (green), oxygen (yellow), and sulfur (cyan) of the vesicle shown in (D) showing diffuse organic matter, Fe,Ni-sulfides, and Ca-sulfate. **(G)** Carbon EEL spectra from molecular carbonate incorporated into phyllosilicates, i.e., clay-bound carbon (CO109-11), an aromatic nanoglobule (A0108-39), an IOM-like nanoglobule (CO109-11), and nanodiamonds (A0108-8). Spectra were acquired at 0.02 eV per channel, and are smoothed to 0.4-eV resolution, after power law background subtraction and arbitrary scaling. **(H)** EDS spectra from molecular carbonate clay-bound carbon (CO109-11; green) and an insoluble organic residue (A0106-9; magenta). The asterisk indicates a Cu background peak from the sample support and microscope.

nebula (37, 38). The insoluble carbonaceous residues contain large nanoglobules and fluffy or porous material, comprising demineralized grain coatings, intergranular material, and small nanoglobules. These microstructures are present in samples from both chambers A and C, and they are consistent in size and shape with those in CI and CM chondrites (28, 34).

Organic nanoglobules have previously been found in early Solar System materials, such as primitive carbonaceous chondrites (39–42), dust particles from Comet Wild 2 (32), IDPs (43), and AMMs (33, 44). The nanoglobules in

Ryugu grains occur in solid and hollow form, typically 50 to 500 nm in diameter, with a few reaching 2000 nm, consistent with nanoglobules in other extraterrestrial materials. The carbon EELS spectra of many of the Ryugu nanoglobules are dominated by an aromatic carbon peak at ~285 eV (Fig. 4G), corresponding to the aromatic-rich carbon-XANES spectra (Fig. 3E). Other prominent peaks are due to aromatic ketone (286.7 eV) and carboxyl (288.5 eV). The fluffy material in the insoluble carbonaceous residues shows these three peaks in varying intensities. The presence of both

aromatic- and IOM-like nanoglobules of various sizes indicates that Ryugu experienced heterogeneous aqueous alteration on its parent body. Correlated STEM-NanoSIMS measurements of a 2000-nm nanoglobule (particle A0108-37; Figs. S6 and S7) show high abundances of aromatic carbon and isotopically anomalous H and N, indicating preservation of material from the interstellar medium or protoplanetary nebula.

The widespread diffuse carbon mixed into phyllosilicates could have been formed from soluble molecules intercalated into clays through oxidation during aqueous alteration (34). Alternatively, the clay-bound diffuse carbon might have been released by hydrolysis of macromolecular organic material during the flow of aqueous fluids (28). The EELS spectra show peaks of either aromatic ketones or aliphatic carbon (287 eV) and carbonate (CO₃ at 290.4 eV) along with aromatic carbon (285 eV) (Fig. 4G). These EELS data are consistent with the carbon-XANES spectrum of the diffuse carbon (Fig. 3, B and E). The relative intensities of the 287-eV and 285-eV peaks vary compared with the 290.4-eV peak. This is consistent with clay-bound organics in CI chondrites (34) but sometimes is a better match to the ungrouped C2 chondrite Tagish Lake (34). In all cases, Mg is detected in the EDS spectra from the clay-bound organic matter (Fig. 4F); however, we cannot determine whether the Mg is associated with the carbonate. We find no evidence for crystalline Mg carbonate in the clay-bound organics, but the CO₃ feature could be associated with molecular CO₃, MgCO₃, or a combination of these.

Pockets of organic matter occur in vesicles inside carbonates (Fig. 4D). A STEM-EDS image (Fig. 4F) shows that this vesicle-bound, diffuse organic matter is associated with phyllosilicates and particles of sulfide and Fe-Ni with sizes of ~10 nm, embedded in a larger grain of calcite. This morphology could indicate carbonate formation from diffuse organic matter. The lack of distinct particle boundaries for the organic matter could indicate it is soluble and therefore potentially lost during our sample preparation, which used ultramicrotomy with a water bath.

We obtained AFM-IR maps of organic inclusions and nanoglobule-like matter at lateral resolutions of 25 and 50 nm. AFM-IR measurements map specific vibrational modes; we used the C=O and C=C modes. Samples from chambers A and C were analyzed using AFM-IR in both tapping and contact modes. Figure 5, A and H, shows combined maps of carbonyl C=O (1720 cm⁻¹, 5.81 μm), aromatic C=C (1600 cm⁻¹, 6.25 μm), and Si-O (1020 cm⁻¹, 9.80 μm) modes. The diffuse organic component within the phyllosilicate matrix is evident in both samples. The maps show small (up to ~100 nm) organic nanoglobule-like inclusions

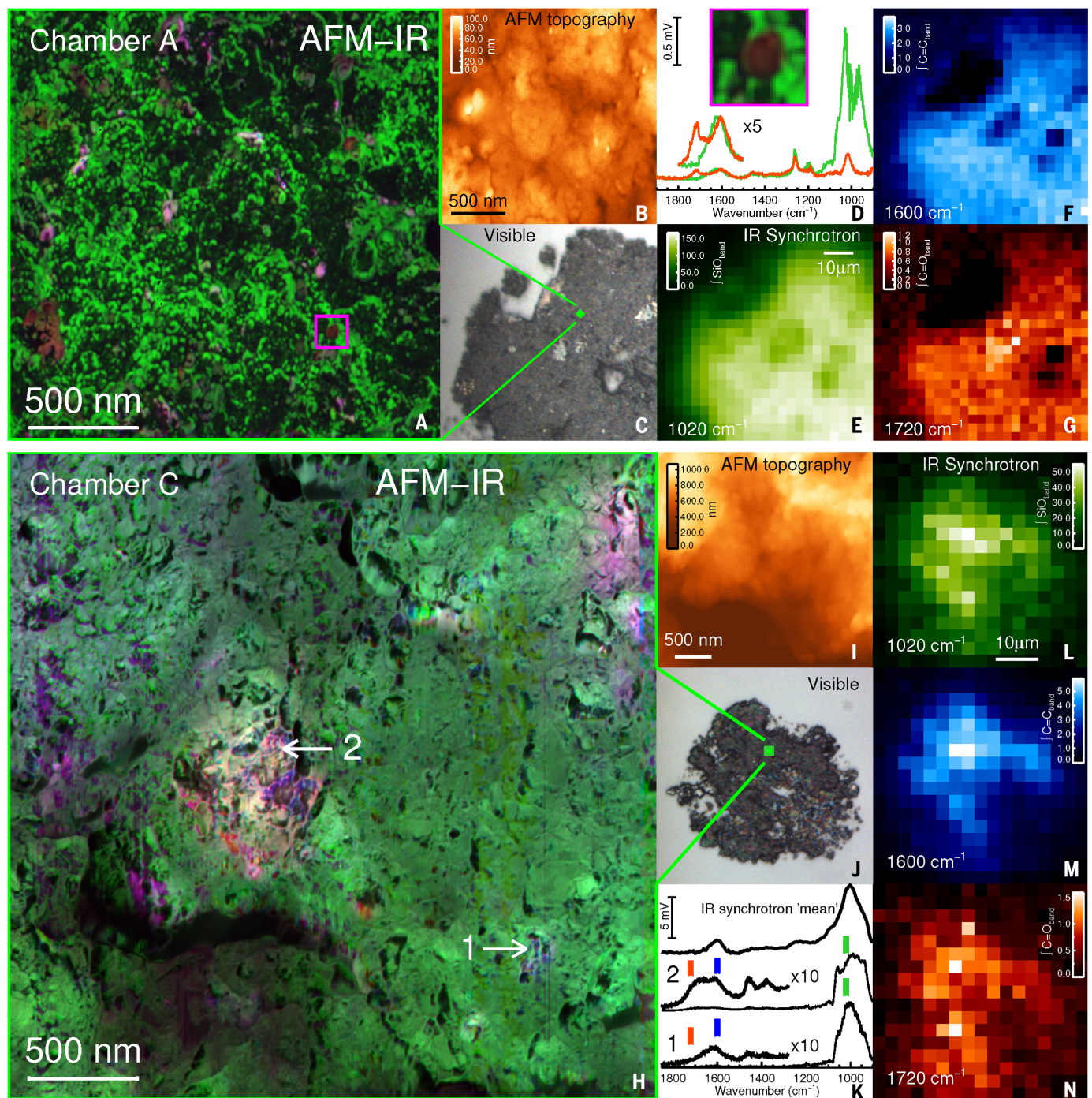


Fig. 5. AFM-IR analysis of intact Ryugu grains A0108 and C0109. (A and H) Composite AFM-IR images of the intact Ryugu grains A0108-15 in tapping mode, 2 μm by 2 μm (A), and C0109-4 in contact mode, 3 μm by 3 μm (H). Colors indicate the C=O (1720 cm^{-1} , 5.81 μm ; red), C=C (1600 cm^{-1} , 6.25 μm ; blue), and Si-O (1020 cm^{-1} , 9.80 μm ; green) peaks. Each image has been normalized to its maximum peak value. Organic matter is widespread throughout each sample. In (A), small organic globules are visible (red-brown) surrounded by a dominant phyllosilicate. The magenta box indicates the inclusion used for (D). (B) AFM topographic map of the 2 μm -by-2 μm area in (A). (C) Visible light image (75 μm by 75 μm) showing the location of the AFM-IR map (green square). (D) AFM-IR spectrum (red) of the globule indicated in (A) and shown in the inset and background spectrum (green) taken in a region 100 nm away. The AFM-IR signal is shown in millivolts, which is proportional to optical depth (11). The C=C and C=O absorptions spectral region is also shown with a $\times 5$ factor for better visibility. (E to

G) Synchrotron FTIR maps of the same 75 μm -by-75 μm area as in (C) of the C=O (1720 cm^{-1} , 5.81 μm ; red) (G), C=C (1600 cm^{-1} , 6.25 μm ; blue) (F), and Si-O (1020 cm^{-1} , 9.80 μm ; green) (E) peaks. Data were acquired with a 6 μm -by-6 μm beam size, sampled with 3- μm steps. Color bars show the integrated optical depths calculated for each band. (H) Organic matter in the Ryugu grain C0109-4 appears as red-purple inclusions standing out from the dominant phyllosilicate signal. Arrows indicate the positions used for the spectra in (K). (I) AFM topographic map of the 3 μm -by-3 μm area. (J) Visible image (51 μm by 51 μm) showing the location of the AFM-IR map (green square). (K) AFM-IR spectra of a C=O-poor region [labeled 1 in (H)] and organic inclusions (labeled 2) compared with the average synchrotron FTIR spectrum. Red, blue, and green tick marks indicate spectral positions corresponding to the AFM-IR images combined in (H). (L to N) Same as [(E) to (G)] but for the 51 μm -by-51 μm region shown in (J). To aid color-blind readers, another version of this figure with alternative colors is provided as fig. S5.

in the chamber A sample (Fig. 5A) and organic inclusions in the chamber C samples (Fig. 5H). The abundances of carbonyl and C=C vary between the organic inclusions. These AFM-IR results are consistent with and complementary to those from STEM-EELS-EDS and STXM-XANES discussed above.

Elemental abundances

The elemental abundances of macromolecular organic matter in meteorites are highly heterogeneous, both between meteorite groups and at the micrometer scale, reflecting the complex histories of these materials (45, 46). We used NanoSIMS to map the H, C, N, O, and S elemental abundances of the Ryugu samples.

The ratios of O/C, N/C, and S/C in the acid-insoluble carbonaceous residues from Ryugu were estimated from NanoSIMS elemental maps of the major isotopes (^{16}O , $^{12}\text{C}^{14}\text{N}$, and ^{32}S) and were compared between samples taken from chambers A and C. The bulk O/C ratio (0.12 ± 0.03) in chamber A was consistent with those of CI (0.15 to 0.18), CM (0.11 to 0.23), and CR chondrites (0.11 to 0.22) (45). The bulk O/C ratio (0.04 ± 0.01) in chamber C was one-third of those values. We cannot determine whether this difference is the result of intrinsic differences between the two sampling sites or heterogeneity within the samples. There are smaller differences in the bulk ratios N/C [0.035 ± 0.006 (A0106); 0.021 ± 0.001 (C0107)] and S/C [0.032 ± 0.001 (A0106); 0.025 ± 0.001 (C0107)] between the two chambers, which are within the ranges of those for CI, CM, and CR chondrites ($0.026 < \text{N/C} < 0.039$ and $0.02 < \text{S/C} < 0.06$) (45).

We also used STEM-EDS to measure N, O, and S abundances, relative to C, at the nano-to-micrometer scale. An EDS spectrum from an $\sim 1\text{-}\mu\text{m}^2$ region of an ultrathin section of carbonaceous residue from chamber A is shown in Fig. 4H. The average compositions measured for carbonaceous residues are $\text{C}_{100}\text{N}_1\text{O}_{10}\text{S}_{0.8}$ for chamber A and $\text{C}_{100}\text{N}_2\text{O}_{10}\text{S}_{0.8}$ for chamber C. The insoluble carbonaceous residues contain some nanoparticulate minerals, including chromite, with varying Al, Mg, and Fe and sulfides with variable Fe, Ni, and (more rarely) CuS. These particles were excluded from the STEM-EDS measurements when >4 nm in size. These nitrogen abundances are slightly lower than the bulk N/C ratio estimated using NanoSIMS and are consistent with the weak nitrogen-XANES absorption of the Ryugu grains.

Isotopic compositions

NanoSIMS was also used to measure the isotopic compositions of H, C, and N. The resulting maps (Fig. 6, A to C) show bulk enrichments of D (^2H) and/or ^{15}N in most analyzed Ryugu particles from aggregates A0108 and C0109, with a high degree of isotopic heterogeneity at the micrometer scale. The NanoSIMS H mea-

surements are dominated by H from the organic matter but also include H in phyllosilicates and possible contamination by terrestrial water. The isotopic compositions are expressed in delta notation: $\delta R = [(R_{\text{sample}}/R_{\text{standard}}) - 1] \times 1000$, where R_{sample} is the isotopic ratio of the sample and R_{standard} is the ratio of a terrestrial standard. The average measured H isotopic compositions (δD) of particles range from $+254 \pm 52$ per mil (‰) to $+490 \pm 100$ ‰ (table S3), consistent with the $\delta\text{D} = +252 \pm 13$ ‰ measured in an analysis of other Ryugu grains with a different technique (47). There is no obvious difference between grains from chambers A and C. The bulk N isotopic compositions $\delta^{15}\text{N} = +39 \pm 5$ to $+43 \pm 4$ ‰ are also within the range reported for other Ryugu grains, measured with different methods [$\delta^{15}\text{N} = +43.0 \pm 9.0$ ‰ (47) and $\delta^{15}\text{N} = 0$ to $+20$ ‰ (48)]. Figure S8 shows that the bulk δD and $\delta^{15}\text{N}$ of the Ryugu grains are between the bulk values of CI chondrites [$\delta\text{D} = +170$ to $+300$ ‰ and $\delta^{15}\text{N} = +39$ to $+52$ ‰ (49)] and IOM in CI chondrites [$\delta\text{D} = \sim +975$ ‰ and $\delta^{15}\text{N} = +31$ ‰ (45)].

Isotopic ratios determined for individual submicrometer- to micrometer-sized carbonaceous grains within the NanoSIMS maps are similar to those of carbonaceous chondrites and IDPs (43, 46). Most grains are consistent with the bulk average, within the uncertainties, whereas a small fraction of outliers have D and/or ^{15}N enrichments or depletions (Fig. 6, D to F), which we term hotspots and coldspots, respectively. These have a similar range of compositions to those seen in CI (46) and CM (50) chondrites but smaller than that seen in CR chondrites (29). There is no correlation between δD and $\delta^{15}\text{N}$ for the hot- or coldspots, and a wide range of compositions occur over small spatial scales (Fig. 6, B and C). The origin(s) of the H and N isotopic anomalies in meteorites are debated; current consensus models propose that they reflect isotopic fractionation at low temperatures in interstellar clouds or the outer protoplanetary nebula (51–54).

The NanoSIMS measurements show that the bulk Ryugu particles, and almost all C-rich particles within them, have $\delta^{13}\text{C}$ values within the range of organic matter in carbonaceous chondrites [$\delta^{13}\text{C} = -35$ to -5 ‰ (45)]. However, $\sim 0.5\%$ of the C-rich particles have ^{13}C enrichments or depletions (Fig. 6G) $>2\sigma$ above or below the bulk values. These particles have a range of $\delta^{13}\text{C}$ and $\delta^{15}\text{N}$ values similar to those seen in organic grains with anomalous carbon isotopes in primitive CM chondrites. For the Ryugu samples, ^{13}C -rich particles have a wider range of $\delta^{15}\text{N}$ values compared with ^{13}C -poor ones, likely reflecting different origins. Two very small (≤ 150 nm) regions have much higher ^{13}C enrichments: $\delta^{13}\text{C} = 700$ and 4800 ‰, which indicates that they are presolar grains

that formed in the outflows of previous generations of stars (55).

The acid-insoluble carbonaceous residues from the Ryugu samples showed bulk D-enrichments [$\delta\text{D} = +306 \pm 42$ ‰ (A0106) and $+440 \pm 52$ ‰ (C0107)] (Fig. 7I) lower than the bulk hydrogen compositions of the IOM in CI chondrites ($\delta\text{D} = +972$ ‰ for Orgueil and $+978$ ‰ for Ivuna) and CM chondrites ($+639$ ‰ $< \delta\text{D} < +893$ ‰) (45). The distributions of D-rich hotspots [distribution modes $\delta\text{D} = +1030$ ‰ (A0106) and $+1374$ ‰ (C0107)] were consistent with CI and CM chondrites but not CR chondrites (56).

The bulk N isotopic compositions of the insoluble carbonaceous residues from Ryugu samples [$\delta^{15}\text{N} = +17.4 \pm 1.9$ ‰ (A0106) and $+30 \pm 4.3$ ‰ (C0107)] (Fig. 7J) are consistent with those of IOM in CI chondrites ($\delta^{15}\text{N} = +30.7$ ‰ for Orgueil and $+31.9$ ‰ for Ivuna) (45). $\delta^{15}\text{N}$ was more heterogeneous in the sample from chamber C than that from chamber A. The ^{15}N -rich hotspots [distribution modes $\delta^{15}\text{N} = +241$ ‰ (A0106) and $+348$ ‰ (C0107)] were within the range of CI and CM carbonaceous chondrites (57). ^{15}N -depleted coldspots ($\delta^{15}\text{N} = -100$ to -380 ‰) were detected. ^{15}N coldspots have previously been reported in the matrices of carbonaceous chondrites (57–59) and IDPs (43) and have been interpreted as indicating organic grains that have been partially equilibrated with protosolar or interstellar N_2 gas (43).

Comparison with D-type asteroids and comets

We compare the organic matter of Ryugu (a C-type asteroid) with other primitive small bodies in the early Solar System. Of the carbonaceous chondrites, the Tagish Lake meteorite is thought to be related to dark (D-type) asteroids, which are mainly located in the outer regions of the asteroid belt and among the trojan asteroids of Jupiter (60). Tagish Lake contains organic and mineralogical variations between different specimens that reflect variable degrees of alteration on the same parent body (61, 62). The ratios D/H, H/C, and aliphatic carbon to aromatic carbon decrease systematically with increasing alteration of the Tagish Lake meteorite samples (61).

We infer that the organic matter in the Ryugu samples has not been heated to temperatures higher than 200°C based on the similarity of its chemical features with primitive carbonaceous CI and CM chondrites. Like the IOM from Orgueil (63) and Murchison (64), the organic macromolecules in the Ryugu samples likely contain polyaromatic structures that are composed of small numbers of aromatic rings with short, cross-linked aliphatic chains and various oxygen- and nitrogen-bearing functional groups. This macromolecular structure is distinct from graphitic or glassy carbon produced by heating: We did not find any evidence

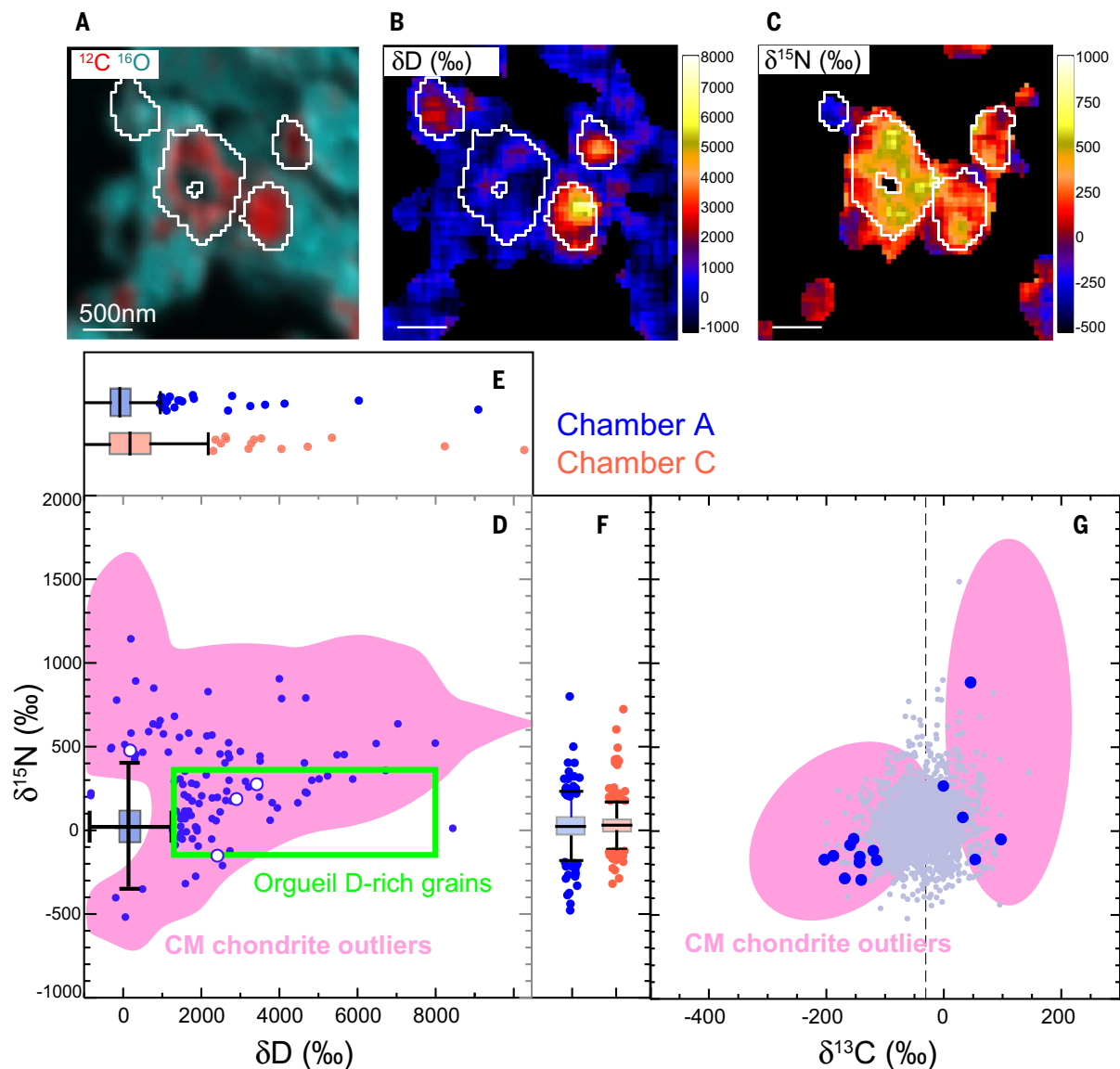


Fig. 6. NanoSIMS analysis of the intact Ryugu grains A0108 and C0109.

(A to C) NanoSIMS images of an ~3 mm-by-3 mm area of a microtome slice from Ryugu grain A0108-11. (A) Map of ^{16}O (cyan) and ^{12}C (red). White outlines indicate four C-rich particles embedded in the silicate matrix. (B and C) Hydrogen (B) and nitrogen (C) isotope abundances of the same region. The ratios vary between the carbonaceous inclusions. (D to F) H and N isotopic ratios for individual C-rich particles [regions of interest (ROIs)] within Ryugu grains. Most ROIs are consistent (within the uncertainties) with the bulk averages; they are represented by box-and-whisker plots, where the box size represents the inner 50% of data around the median [interquartile range (IQR)] and the whiskers indicate the ± 1.5 IQR range beyond that. Dots indicate outliers beyond those ranges (hotspots and coldspots)

from A0108 (blue) and C0109 (orange). In (D), white dots indicate the grains shown in (A) to (C), and the error bar is 1σ . The distributions of H and N isotope ratios are consistent between (D) and those in (E) and (F) (acquired in different laboratories) and between the two Ryugu samples. The pink shaded region indicates the ranges of H and N hotspots and coldspots in primitive CM chondrite meteorites (50), and the green box indicates the ranges seen in CI chondrite Orgueil (46). The Ryugu outliers span a similar range to that of the CI and CM chondrites. (G) $\delta^{15}\text{N}$ as a function of $\delta^{13}\text{C}$ for the Ryugu grain A0109. The gray points indicate all C-rich ROIs, whereas blue circles are outliers ($>2\sigma$ away from bulk average). The pink region is the same as in (D). The Ryugu outliers span a similar range to that seen in CM chondrites. The dashed vertical line indicates the bulk $\delta^{13}\text{C}$ of CI chondrite IOM.

of highly conjugated sp^2 carbon. Laboratory experiments have shown that aliphatic carbon in IOM from primitive carbonaceous chondrites is reduced after hydrous heating at 300°C for 6 days (65). Therefore, the higher abundance of aliphatic carbon in the organic residue of Ryugu—compared with that of primitive carbonaceous chondrites—indicates that the Ryugu grains did not experience short heating equivalent to the experimental conditions.

The distribution of organic functional groups present in the Ryugu samples is unlike aqueously altered carbonaceous chondrites, for which organic particles and nanoglobules show predominantly IOM-like XANES spectra with only occasional highly aromatic grains (28, 30, 66). Ryugu samples contain abundant aromatic-rich particles and nanoglobules, a high abundance of IOM-like diffuse carbon in matrix, and molecular carbonate associated with phyl-

losilicates. Progressive aqueous alteration in situ causes (i) an increase in the amount of diffuse organic matter associated with matrix phyllosilicates, (ii) an increase in the proportion of aromatic and oxygen-bearing functional groups in discrete organic particles and nanoglobules, and (iii) an increase in the variety of XANES spectral features. On the basis of these trends, much of the internal spectral variation in the Ryugu samples, including carbon grains with

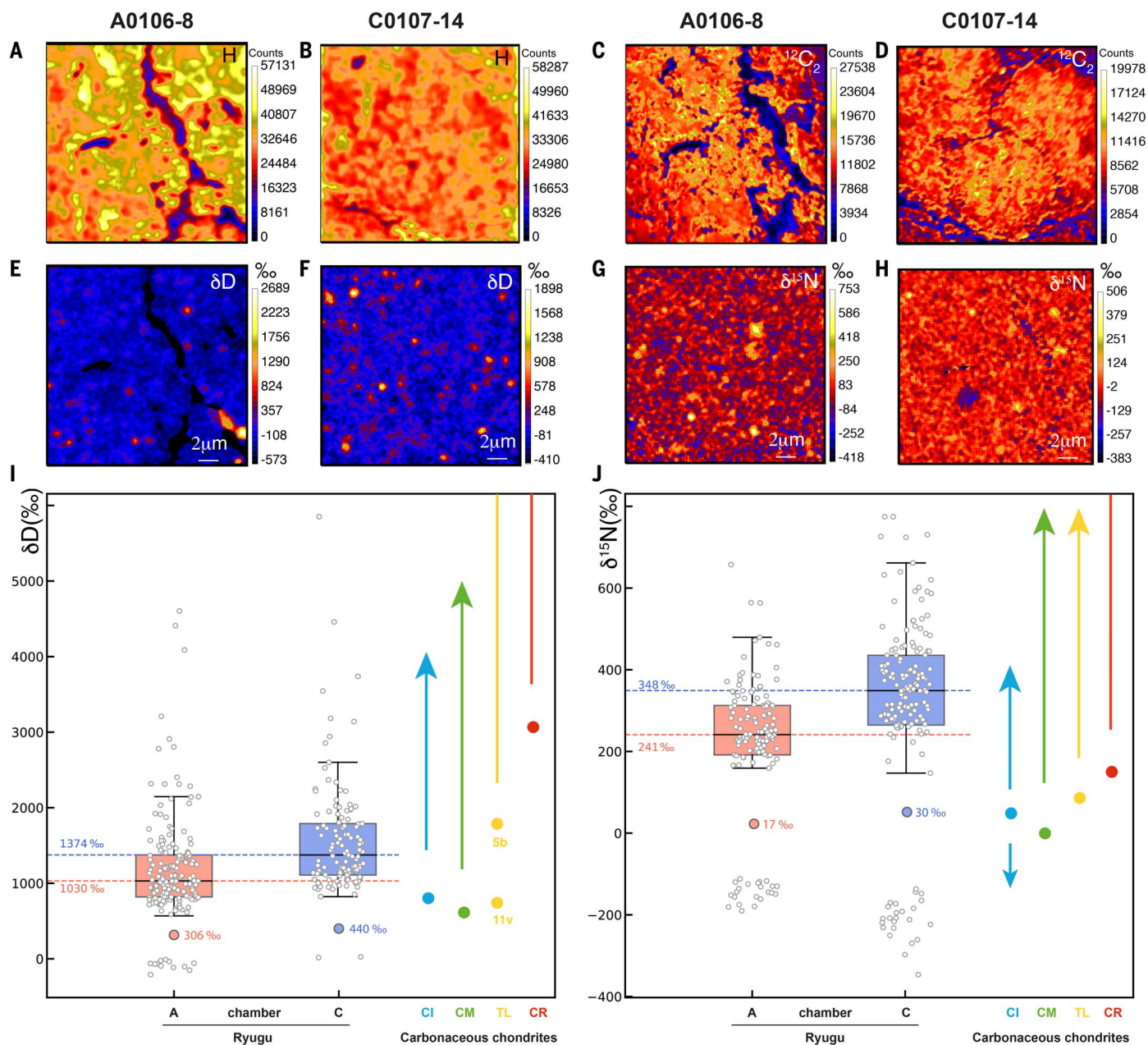


Fig. 7. NanoSIMS analysis of insoluble carbonaceous residues from Ryugu grains A0106 and C0107. (A to D) Hydrogen [(A) and (B)] and carbon [(C) and (D)] maps for insoluble carbonaceous residues of A0106 and C0107, respectively, acquired at the same locations. (E to H) The corresponding H [(E) and (F)] and N [(G) and (H)] isotope ratio maps show numerous micrometer-sized D-rich and ^{15}N -rich hotspots. The carbon and hydrogen images indicate that these hotspots consist of organic carbon. (I and J) Hydrogen (I) and nitrogen (J) box plot diagrams showing the distributions of isotope ratios in the insoluble carbonaceous residues A0106-8 (orange) and C0107-14 (blue). Open gray circles show hotspots (or

coldspots), micrometer-sized areas with isotope ratios much higher (or lower) than the average composition. Large orange and blue circles indicate the bulk average value for each residue. Horizontal dashed lines indicate the mode of each distribution of hotspots. Data for the IOM of CI (light blue), CM (green), CR (red), and Tagish Lake (yellow) chondrites are shown for comparison. Filled circles are bulk values (45); for Tagish Lake, subsamples 5b (less altered) and 11v (altered) (61) are shown separately. Upward-pointing arrows (some extend beyond the plot) indicate the range of hotspots reported for those meteorites (46, 56, 57). For Orgueil, the downward arrow indicates the extent of ^{15}N -depleted coldspots.

an aromatic XANES spectral shape (Fig. 3E), likely developed through redistribution of organic matter and formation of additional organic molecules during aqueous alteration on the parent body rather than preaccretionary diversity inherited from the protosolar molecular cloud. Carbonaceous grains and nano-

globules with highly aromatic XANES spectra (not aromatic spectra; Fig. 3E) provide a possible exception to this proposal. These highly aromatic grains are more likely to represent original accreted materials because similar XANES spectra have been found in unaltered, petrologic type 3 carbonaceous chondrites (30)

and in cometary dust particles (32). This is consistent with our observation of a large, highly aromatic nanoglobule containing D and ^{15}N isotopic anomalies (figs. S6 and S7).

The δD distributions of the C-rich particles in the Ryugu grains are consistent with those in the Tagish Lake meteorite (56) and CI and

CM chondrites (46, 57). The δD distributions of the Ryugu insoluble carbonaceous residues from chambers A and C are within the ranges of IOMs in the most and least altered fragments of Tagish Lake, respectively (61). The hydrogen isotopic variations among the different lithologies of Tagish Lake have previously been explained by depletion of D through hydrogen isotopic exchange or hydrolysis of D-rich structures of IOM during various degrees of planetesimal hydrothermal alteration (65, 67). By contrast, the δD distributions of our Ryugu samples are lower than those of less-altered CR chondrites (56), the most primitive class of IDPs (68), and comet-derived AMMs (33, 69). We therefore propose that Ryugu organic matter is a product of heterogeneous aqueous processing, which occurred on both C- and D-type asteroids, of the common primordial materials formed at an earlier stage of the solar nebula. The $\delta^{15}N$ distributions of the intact grains and insoluble residues from our Ryugu samples were within the ranges of C-rich particles (39, 56) and IOM (bulk) (61) in Tagish Lake and Comet Wild 2 (32) as well as CI and CM chondrites. However, they are lower than the $\delta^{15}N$ distributions of anhydrous IDPs (43, 68) and the IOM from CR chondrites (56). Nitrogen isotopic compositions are less affected than hydrogen isotopes by modification through parent body processes (45, 57, 61, 66), and their variations indicate mixing of different isotopic components from different precursors (53).

Nitrogen content can be an indicator of chemical evolution in the early Solar System. The measured N abundance (N/C = 0.01 to 0.035) of the insoluble carbonaceous residue in Ryugu samples is similar to that in primitive carbonaceous chondrites (45) and consistent with the total bulk N abundance (~0.15 wt %) (47). The N/C ratio of IOM from Tagish Lake (~0.042) is higher than those of the Ryugu samples. By contrast, some cometary materials, such as dust particles from Comet Wild 2, anhydrous AMMs, and ultracarbonaceous AMMs (UCAMMs), contain N-rich organics [N/C = 0.07 to 0.24 (32, 44, 70)]. Those are composed of a variety of nitrogen-bearing functional groups, such as imine, nitrile and/or heterocyclic N, or amide (32, 33, 44, 70, 71). The N contents of Comet 67P/Churyumov-Gerasimenko particles were heterogeneous (N/C = 0.018 to 0.06) (72) but lower than the N/C ratio of the Sun (0.3 ± 0.1) (73). The depletion of N in that comet might be because of the presence of ammonium salts (74, 75). These variations in N/C between different Solar System objects could arise from partitioning between gas and solid phases in the cold interstellar cloud or outer solar nebula or from exposure to the warmer inner Solar System during perihelion passage (74) rather than from processing in the interiors of planet-

esimals. Experiments simulating parent-body aqueous alteration show the N/C ratios in meteoritic IOMs are not substantially modified (65, 76). We therefore conclude that the N abundance in Ryugu macromolecular organic matter is intrinsic—not the product of extensive parent-body processing.

Conclusions

Our analysis of Ryugu samples indicates a direct link between macromolecular organic matter in C-type asteroids and that in primitive carbonaceous chondrites. The observed similarities and variations in molecular, isotopic, and morphological compositions between the Ryugu samples and other Solar System materials indicate a continuum of source material in the solar nebula, which was incorporated into C-type asteroids, D-type asteroids, and comets in the early Solar System. Macromolecular organic matter in the surface grains of asteroid Ryugu reflects various degrees of parent-body aqueous alteration and localized preservation of inherited nebular or molecular cloud history. The highly variable nature of the material indicates that the Ryugu organic matter is likely derived from material that was not subjected to long-term space weathering and was only recently exposed to the asteroid surface. The macromolecular organic matter shows no record of high-temperature impact heating of Ryugu, despite the asteroid being a rubble-pile body formed from impact debris and geomorphological evidence that it experienced subsequent impact cratering (2, 3). This observation is consistent with the homogeneous reflectance spectra of Ryugu's surface (3).

Ryugu materials are much darker than those from primitive carbonaceous chondrites, despite having similar carbon contents (23, 47), so some other factor (or factors) must determine the albedo. Possibilities include the macromolecular organic matter mixed with phyllosilicates (as discussed in this study) or nanophase sulfides (24), both of which have high light absorption efficiency owing to their small grain sizes. Such major, complex aromatic macromolecules in C- and/or D-type asteroids could have supplied the organic inventory and prebiotic molecules (47) that contributed to making Earth a habitable planet.

REFERENCES AND NOTES

1. S. Tachibana *et al.*, Hayabusa2: Scientific importance of samples returned from C-type near-Earth asteroid (162173) 1999 JU₃. *Geochim. J.* **48**, 571–587 (2014). doi: [10.2343/geochemj.2.0350](https://doi.org/10.2343/geochemj.2.0350)
2. S. Watanabe *et al.*, Hayabusa2 arrives at the carbonaceous asteroid 162173 Ryugu—A spinning top-shaped rubble pile. *Science* **364**, 268–272 (2019). doi: [10.1126/science.aaw8032](https://doi.org/10.1126/science.aaw8032); pmid: 30890588
3. S. Sugita *et al.*, The geomorphology, color, and thermal properties of Ryugu: Implications for parent-body processes. *Science* **364**, eaaw0422 (2019). doi: [10.1126/science.aaw0422](https://doi.org/10.1126/science.aaw0422); pmid: 30890587

4. K. Kitazato *et al.*, The surface composition of asteroid 162173 Ryugu from Hayabusa2 near-infrared spectroscopy. *Science* **364**, 272–275 (2019). doi: [10.1126/science.aaw7432](https://doi.org/10.1126/science.aaw7432); pmid: 30890589
5. T. Morota *et al.*, Sample collection from asteroid (162173) Ryugu by Hayabusa2: Implications for surface evolution. *Science* **368**, 654–659 (2020). doi: [10.1126/science.aaz6306](https://doi.org/10.1126/science.aaz6306); pmid: 32381723
6. N. Sakatani *et al.*, Anomalous porous boulders on (162173) Ryugu as primordial materials from its parent body. *Nat. Astron.* **5**, 766–774 (2021). doi: [10.1038/s41550-021-01371-7](https://doi.org/10.1038/s41550-021-01371-7)
7. E. Tatsumi *et al.*, Spectrally blue hydrated parent body of asteroid (162173) Ryugu. *Nat. Commun.* **12**, 5837 (2021). doi: [10.1038/s41467-021-26071-8](https://doi.org/10.1038/s41467-021-26071-8); pmid: 34611167
8. E. Tatsumi *et al.*, Collisional history of Ryugu's parent body from bright surface boulders. *Nat. Astron.* **5**, 39–45 (2021). doi: [10.1038/s41550-020-1179-z](https://doi.org/10.1038/s41550-020-1179-z)
9. T. Yada *et al.*, Preliminary analysis of the Hayabusa2 samples returned from C-type asteroid Ryugu. *Nat. Astron.* **6**, 214–220 (2021). doi: [10.1038/s41550-021-01550-6](https://doi.org/10.1038/s41550-021-01550-6)
10. C. Pilorget *et al.*, First compositional analysis of Ryugu samples by the MicroOmega hyperspectral microscope. *Nat. Astron.* **6**, 221–225 (2021). doi: [10.1038/s41550-021-01549-z](https://doi.org/10.1038/s41550-021-01549-z)
11. Materials and methods are available as supplementary materials.
12. S. Tachibana *et al.*, Pebbles and sand on asteroid (162173) Ryugu: In situ observation and particles returned to Earth. *Science* **375**, 1011–1016 (2022). doi: [10.1126/science.abj8624](https://doi.org/10.1126/science.abj8624); pmid: 35143255
13. L. Bonal, E. Quirico, M. Bourot-Denise, G. Montagnac, Determination of the petrologic type of CV3 chondrites by Raman spectroscopy of included organic matter. *Geochim. Cosmochim. Acta* **70**, 1849–1863 (2006). doi: [10.1016/j.gca.2005.12.004](https://doi.org/10.1016/j.gca.2005.12.004)
14. H. Busemann, C. M. O'D. Alexander, L. R. Nittler, Characterization of insoluble organic matter in primitive meteorites by microRaman spectroscopy. *Meteorit. Planet. Sci.* **42**, 1387–1416 (2007). doi: [10.1111/j.1945-5100.2007.tb00581.x](https://doi.org/10.1111/j.1945-5100.2007.tb00581.x)
15. L. Bonal, E. Quirico, L. Flandinet, G. Montagnac, Thermal history of type 3 chondrites from the Antarctic meteorite collection determined by Raman spectroscopy of their polyaromatic carbonaceous matter. *Geochim. Cosmochim. Acta* **189**, 312–337 (2016). doi: [10.1016/j.gca.2016.06.017](https://doi.org/10.1016/j.gca.2016.06.017)
16. E. Quirico *et al.*, Prevalence and nature of heating processes in CM and C2-ungrouped chondrites as revealed by insoluble organic matter. *Geochim. Cosmochim. Acta* **241**, 17–37 (2018). doi: [10.1016/j.gca.2018.08.029](https://doi.org/10.1016/j.gca.2018.08.029)
17. G. R. Huss, A. E. Rubin, J. N. Grossman, in *Meteorites and the Early Solar System II*, D. S. Lauretta, H. Y. McSween, Eds. (Univ. Arizona Press, 2006), pp. 567–586.
18. T. Nakamura, Yamato 793321 CM chondrite: Dehydrated regolith material of a hydrous asteroid. *Earth Planet. Sci. Lett.* **242**, 26–38 (2006). doi: [10.1016/j.epsl.2005.11.040](https://doi.org/10.1016/j.epsl.2005.11.040)
19. T. Osawa, H. Kagi, T. Nakamura, T. Noguchi, Infrared spectroscopic taxonomy for carbonaceous chondrites from speciation of hydrous components. *Meteorit. Planet. Sci.* **40**, 71–86 (2005). doi: [10.1111/j.1945-5100.2005.tb00365.x](https://doi.org/10.1111/j.1945-5100.2005.tb00365.x)
20. Y. Kebukawa, C. M. O'D. Alexander, G. D. Cody, Comparison of FT-IR spectra of bulk and acid insoluble organic matter in chondritic meteorites: An implication for missing carbon during demineralization. *Meteorit. Planet. Sci.* **54**, 1632–1641 (2019). doi: [10.1111/maps.13302](https://doi.org/10.1111/maps.13302)
21. P. Beck *et al.*, Hydrous mineralogy of CM and CI chondrites from infrared spectroscopy and their relationship with low albedo asteroids. *Geochim. Cosmochim. Acta* **74**, 4881–4892 (2010). doi: [10.1016/j.gca.2010.05.020](https://doi.org/10.1016/j.gca.2010.05.020)
22. D. Takir *et al.*, Nature and degree of aqueous alteration in CM and CI carbonaceous chondrites. *Meteorit. Planet. Sci.* **48**, 1618–1637 (2013). doi: [10.1111/maps.12171](https://doi.org/10.1111/maps.12171)
23. T. Yokoyama *et al.*, Samples returned from the asteroid Ryugu are similar to Ivuna-type carbonaceous meteorites. *Science* **379**, eabn7850 (2023). doi: [10.1126/science.abn7850](https://doi.org/10.1126/science.abn7850)
24. T. Nakamura *et al.*, Formation and evolution of carbonaceous asteroid Ryugu: Direct evidence from returned samples. *Science* **379**, eabn8671 (2023). doi: [10.1126/science.abn8671](https://doi.org/10.1126/science.abn8671)
25. M. Gounelle, M. E. Zolensky, The Orgueil meteorite: 150 years of history. *Meteorit. Planet. Sci.* **49**, 1769–1794 (2014). doi: [10.1111/maps.12351](https://doi.org/10.1111/maps.12351)
26. Y. Kebukawa, C. M. O'D. Alexander, G. D. Cody, Compositional diversity in insoluble organic matter in type 1, 2 and 3 chondrites as detected by infrared spectroscopy. *Geochim. Cosmochim. Acta* **75**, 3530–3541 (2011). doi: [10.1016/j.gca.2011.03.037](https://doi.org/10.1016/j.gca.2011.03.037)

27. F.-R. Orthous-Daunay *et al.*, Mid-infrared study of the molecular structure variability of insoluble organic matter from primitive chondrites. *Icarus* **223**, 534–543 (2013). doi: [10.1016/j.icarus.2013.01.003](https://doi.org/10.1016/j.icarus.2013.01.003)
28. C. Le Guillou, S. Bernard, A. J. Brearley, L. Remusat, Evolution of organic matter in Orgueil, Murchison and Renazzo during parent body aqueous alteration: In situ investigations. *Geochim. Cosmochim. Acta* **131**, 368–392 (2016). doi: [10.1016/j.gca.2013.11.020](https://doi.org/10.1016/j.gca.2013.11.020)
29. L. R. Nittler *et al.*, A cometary building block in a primitive asteroidal meteorite. *Nat. Astron.* **3**, 659–666 (2019). doi: [10.1038/s41550-019-0737-8](https://doi.org/10.1038/s41550-019-0737-8)
30. B. T. De Gregorio *et al.*, Isotopic and chemical variation of organic nanoglobules in primitive meteorites. *Meteorit. Planet. Sci.* **48**, 904–928 (2013). doi: [10.1111/maps.12109](https://doi.org/10.1111/maps.12109)
31. L. P. Keller *et al.*, The nature of molecular cloud material in interplanetary dust. *Geochim. Cosmochim. Acta* **68**, 2577–2589 (2004). doi: [10.1016/j.gca.2003.10.044](https://doi.org/10.1016/j.gca.2003.10.044)
32. B. T. De Gregorio *et al.*, Isotopic anomalies in organic nanoglobules from Comet 81P/Wild 2: Comparison to Murchison nanoglobules and isotopic anomalies induced in terrestrial organics by electron irradiation. *Geochim. Cosmochim. Acta* **74**, 4454–4470 (2010). doi: [10.1016/j.gca.2010.05.010](https://doi.org/10.1016/j.gca.2010.05.010)
33. T. Noguchi *et al.*, Variation of mineralogy and organic material during the early stages of aqueous activity recorded in Antarctic micrometeorites. *Geochim. Cosmochim. Acta* **208**, 119–144 (2017). doi: [10.1016/j.gca.2017.03.034](https://doi.org/10.1016/j.gca.2017.03.034)
34. L. A. J. Garvie, P. R. Buseck, Prebiotic carbon in clays from Orgueil and Ivuna (Cl), and Tagish Lake (C2 ungrouped) meteorites. *Meteorit. Planet. Sci.* **42**, 2111–2117 (2007). doi: [10.1111/j.1945-5100.2007.tb01011.x](https://doi.org/10.1111/j.1945-5100.2007.tb01011.x)
35. G. D. Cody *et al.*, Organic thermometry for chondritic parent bodies. *Earth Planet. Sci. Lett.* **272**, 446–455 (2008). doi: [10.1016/j.epsl.2008.05.008](https://doi.org/10.1016/j.epsl.2008.05.008)
36. C. M. O'D. Alexander, G. D. Cody, B. T. De Gregorio, L. R. Nittler, R. M. Stroud, The nature, origin and modification of insoluble organic matter in chondrites, the major source of Earth's C and N. *Chem. Erde* **77**, 227–256 (2017). doi: [10.1016/j.chemer.2017.01.007](https://doi.org/10.1016/j.chemer.2017.01.007); pmid: [31020720](https://pubmed.ncbi.nlm.nih.gov/31020720/)
37. D. D. Clayton, Origin of heavy xenon in meteoritic diamonds. *Astrophys. J.* **340**, 613–619 (1989). doi: [10.1086/167422](https://doi.org/10.1086/167422)
38. Z. R. Dai *et al.*, Possible in situ formation of meteoritic nanodiamonds in the early Solar System. *Nature* **418**, 157–159 (2002). doi: [10.1038/nature00897](https://doi.org/10.1038/nature00897); pmid: [12110882](https://pubmed.ncbi.nlm.nih.gov/12110882/)
39. K. Nakamura-Messenger, S. Messenger, L. P. Keller, S. J. Clemett, M. E. Zolensky, Organic globules in the Tagish Lake meteorite: Remnants of the protosolar disk. *Science* **314**, 1439–1442 (2006). doi: [10.1126/science.1132175](https://doi.org/10.1126/science.1132175); pmid: [17138898](https://pubmed.ncbi.nlm.nih.gov/17138898/)
40. T. Matsumoto *et al.*, Three-dimensional observation and morphological analysis of organic nanoglobules in a carbonaceous chondrite using X-ray micro-tomography. *Geochim. Cosmochim. Acta* **116**, 84–95 (2013). doi: [10.1016/j.gca.2012.05.007](https://doi.org/10.1016/j.gca.2012.05.007)
41. M. Hashiguchi, S. Kobayashi, H. Yurimoto, In situ observation of D-rich carbonaceous globules embedded in NWA 801 CR2 chondrite. *Geochim. Cosmochim. Acta* **122**, 306–323 (2013). doi: [10.1016/j.gca.2013.08.007](https://doi.org/10.1016/j.gca.2013.08.007)
42. C. Le Guillou, A. Brearley, Relationships between organics, water and early stages of aqueous alteration in the pristine CR3.0 chondrite MET 00426. *Geochim. Cosmochim. Acta* **131**, 344–367 (2014). doi: [10.1016/j.gca.2013.10.024](https://doi.org/10.1016/j.gca.2013.10.024)
43. G. Matrajt, S. Messenger, D. Brownlee, D. Joswiak, Diverse forms of primordial organic matter identified in interplanetary dust particles. *Meteorit. Planet. Sci.* **47**, 525–549 (2012). doi: [10.1111/j.1945-5100.2011.01310.x](https://doi.org/10.1111/j.1945-5100.2011.01310.x)
44. H. Yabuta *et al.*, Formation of an ultracarbonaceous Antarctic micrometeorite through minimal aqueous alteration in a small porous icy body. *Geochim. Cosmochim. Acta* **214**, 172–190 (2017). doi: [10.1016/j.gca.2017.06.047](https://doi.org/10.1016/j.gca.2017.06.047)
45. C. M. O'D. Alexander, M. Fogel, H. Yabuta, G. D. Cody, The origin and evolution of chondrites recorded in the elemental and isotopic compositions of their macromolecular organic matter. *Geochim. Cosmochim. Acta* **71**, 4380–4403 (2007). doi: [10.1016/j.gca.2007.06.052](https://doi.org/10.1016/j.gca.2007.06.052)
46. L. Remusat, Y. Guan, Y. Wang, J. M. Eiler, Accretion and preservation of D-rich organic particles in carbonaceous chondrites: Evidence for important transport in the early Solar System nebula. *Astrophys. J.* **713**, 1048–1058 (2010). doi: [10.1088/0004-637X/713/2/1048](https://doi.org/10.1088/0004-637X/713/2/1048)
47. H. Naraoka *et al.*, Soluble organic molecules in samples of the carbonaceous asteroid (162173) Ryugu. *Science* **379**, eabn9033 (2023). doi: [10.1126/science.abn9033](https://doi.org/10.1126/science.abn9033)
48. R. Okazaki *et al.*, Noble gases and nitrogen in samples of asteroid Ryugu record its volatile sources and recent surface evolution. *Science* **379**, eabo0431 (2023). doi: [10.1126/science.abo0431](https://doi.org/10.1126/science.abo0431)
49. J. F. Kerridge, Carbon, hydrogen and nitrogen in carbonaceous chondrites: Abundances and isotopic compositions in bulk samples. *Geochim. Cosmochim. Acta* **49**, 1707–1714 (1985). doi: [10.1016/0016-7037\(85\)90141-3](https://doi.org/10.1016/0016-7037(85)90141-3); pmid: [11539652](https://pubmed.ncbi.nlm.nih.gov/11539652/)
50. L. R. Nittler, C. M. O'D. Alexander, M. J. Verdier-Paoletti, paper presented at the 84th Annual Meeting of the Meteoritical Society, Chicago, IL, 15 to 21 August 2021.
51. Y. Aikawa, G. J. van Zadelhoff, E. F. van Dishoeck, E. Herbst, Warm molecular layers in protoplanetary disks. *Astron. Astrophys.* **386**, 622–632 (2002). doi: [10.1051/0004-6361/20020037](https://doi.org/10.1051/0004-6361/20020037)
52. N. Watanabe, A. Kouchi, Ice surface reactions: A key to chemical evolution in space. *Prog. Surf. Sci.* **83**, 439–489 (2008). doi: [10.1016/j.progsurf.2008.10.001](https://doi.org/10.1016/j.progsurf.2008.10.001)
53. J. Aléon, Multiple origins of nitrogen isotopic anomalies in meteorites and comets. *Astrophys. J.* **722**, 1342–1351 (2010). doi: [10.1088/0004-637X/722/2/1342](https://doi.org/10.1088/0004-637X/722/2/1342)
54. R. Terzieva, E. Herbst, The possibility of nitrogen isotopic fractionation in interstellar clouds. *Mon. Not. R. Astron. Soc.* **317**, 563–568 (2000). doi: [10.1046/j.1365-8711.2000.03618.x](https://doi.org/10.1046/j.1365-8711.2000.03618.x)
55. E. K. Zinner, in *Meteorites, Comets, and Planets*, A. M. Davis, Ed. (Elsevier, 2005), pp. 17–39.
56. H. Busemann *et al.*, Interstellar chemistry recorded in organic matter from primitive meteorites. *Science* **312**, 727–730 (2006). doi: [10.1126/science.1123878](https://doi.org/10.1126/science.1123878); pmid: [16675696](https://pubmed.ncbi.nlm.nih.gov/16675696/)
57. L. Remusat, J.-Y. Bonnet, S. Bernard, A. Buch, E. Quirico, Molecular and isotopic behavior of insoluble organic matter of the Orgueil meteorite upon heating. *Geochim. Cosmochim. Acta* **263**, 235–247 (2019). doi: [10.1016/j.gca.2019.07.013](https://doi.org/10.1016/j.gca.2019.07.013)
58. C. Floss, F. Stadermann, Auger nanoprobe analysis of presolar ferromagnesian silicate grains from primitive CR chondrites QUE 99177 and MET 00426. *Geochim. Cosmochim. Acta* **73**, 2415–2440 (2009). doi: [10.1016/j.gca.2009.01.033](https://doi.org/10.1016/j.gca.2009.01.033)
59. C. Vollmer *et al.*, A primordial ¹⁵N-depleted organic component detected within the carbonaceous chondrite Maribo. *Sci. Rep.* **10**, 20251 (2020). doi: [10.1038/s41598-020-77190-z](https://doi.org/10.1038/s41598-020-77190-z); pmid: [33219224](https://pubmed.ncbi.nlm.nih.gov/33219224/)
60. T. Hiroi, M. E. Zolensky, C. M. Pieters, The Tagish Lake meteorite: A possible sample from a D-type asteroid. *Science* **293**, 2234–2236 (2001). doi: [10.1126/science.1063734](https://doi.org/10.1126/science.1063734); pmid: [11520950](https://pubmed.ncbi.nlm.nih.gov/11520950/)
61. C. D. K. Herd *et al.*, Origin and evolution of prebiotic organic matter as inferred from the Tagish Lake meteorite. *Science* **332**, 1304–1307 (2011). doi: [10.1126/science.1203290](https://doi.org/10.1126/science.1203290); pmid: [21659601](https://pubmed.ncbi.nlm.nih.gov/21659601/)
62. C. M. Gilmour, C. D. K. Herd, P. Beck, Water abundance in the Tagish Lake meteorite from TGA and IR spectroscopy: Evaluation of aqueous alteration. *Meteorit. Planet. Sci.* **54**, 1951–1972 (2019). doi: [10.1111/maps.13362](https://doi.org/10.1111/maps.13362)
63. A. Gardinier *et al.*, Solid state CP/MAS ¹³C NMR of the insoluble organic matter of the Orgueil and Murchison meteorites: Quantitative study. *Earth Planet. Sci. Lett.* **184**, 9–21 (2000). doi: [10.1016/S0012-821X\(00\)00300-9](https://doi.org/10.1016/S0012-821X(00)00300-9)
64. G. D. Cody, C. M. O'D. Alexander, F. Tera, Solid-state (¹H and ¹³C) nuclear magnetic resonance spectroscopy of insoluble organic residue in the Murchison meteorite: A self-consistent quantitative analysis. *Geochim. Cosmochim. Acta* **66**, 1851–1865 (2002). doi: [10.1016/S0016-7037\(01\)00888-2](https://doi.org/10.1016/S0016-7037(01)00888-2)
65. H. Yabuta, L. B. Williams, G. D. Cody, C. M. O'D. Alexander, S. Pizzarello, The insoluble carbonaceous material of CM chondrites: A possible source of discrete organic compounds under hydrothermal conditions. *Meteorit. Planet. Sci.* **42**, 37–48 (2007). doi: [10.1111/j.1945-5100.2007.tb00216.x](https://doi.org/10.1111/j.1945-5100.2007.tb00216.x)
66. V. Vinogradoff *et al.*, Paris vs. Murchison: Impact of hydrothermal alteration on organic matter in CM chondrites. *Geochim. Cosmochim. Acta* **212**, 234–252 (2017). doi: [10.1016/j.gca.2017.06.009](https://doi.org/10.1016/j.gca.2017.06.009)
67. Y. Oba, H. Naraoka, Elemental and isotope behavior of macromolecular organic matter from CM chondrites during hydrous pyrolysis. *Meteorit. Planet. Sci.* **44**, 943–953 (2009). doi: [10.1111/j.1945-5100.2009.tb00779.x](https://doi.org/10.1111/j.1945-5100.2009.tb00779.x)
68. S. Messenger, Identification of molecular-cloud material in interplanetary dust particles. *Nature* **404**, 968–971 (2000). doi: [10.1038/35010053](https://doi.org/10.1038/35010053); pmid: [10801119](https://pubmed.ncbi.nlm.nih.gov/10801119/)
69. J. Duprat *et al.*, Extreme deuterium excesses in ultracarbonaceous micrometeorites from central Antarctic snow. *Science* **328**, 742–745 (2010). doi: [10.1126/science.1184832](https://doi.org/10.1126/science.1184832); pmid: [20448182](https://pubmed.ncbi.nlm.nih.gov/20448182/)
70. G. D. Cody *et al.*, Quantitative organic and light-element analysis of comet 81P/Wild 2 particles using C-, N-, and O-¹⁸-XANES. *Meteorit. Planet. Sci.* **43**, 353–365 (2008). doi: [10.1111/j.1945-5100.2008.tb00627.x](https://doi.org/10.1111/j.1945-5100.2008.tb00627.x)
71. E. Dartois *et al.*, Ultracarbonaceous Antarctic micrometeorites, probing the Solar System beyond the nitrogen snow-line. *Icarus* **224**, 243–252 (2013). doi: [10.1016/j.icarus.2013.03.002](https://doi.org/10.1016/j.icarus.2013.03.002)
72. N. Fray *et al.*, Nitrogen-to-carbon atomic ratio measured by COSIMA in the particles of comet 67P/Churyumov–Gerasimenko. *Mon. Not. R. Astron. Soc.* **469**, S506–S516 (2017). doi: [10.1093/mnras/stx2002](https://doi.org/10.1093/mnras/stx2002)
73. K. Lodders, in *Principles and Perspectives in Cosmochemistry*, A. Goswami, B. E. Reddy, Eds. (Springer, 2010), pp. 379–417.
74. O. Poch *et al.*, Ammonium salts are a reservoir of nitrogen on a cometary nucleus and possibly on some asteroids. *Science* **367**, eaaw7462 (2020). doi: [10.1126/science.aaw7462](https://doi.org/10.1126/science.aaw7462); pmid: [32165559](https://pubmed.ncbi.nlm.nih.gov/32165559/)
75. K. Altwegg *et al.*, Evidence of ammonium salts in comet 67P as explanation for the nitrogen depletion in cometary comae. *Nat. Astron.* **4**, 533–540 (2020). doi: [10.1038/s41550-019-0991-9](https://doi.org/10.1038/s41550-019-0991-9)
76. H. Naraoka *et al.*, A chemical sequence of macromolecular organic matter in the CM chondrites. *Meteorit. Planet. Sci.* **39**, 401–406 (2004). doi: [10.1111/j.1945-5100.2004.tb00101.x](https://doi.org/10.1111/j.1945-5100.2004.tb00101.x)

ACKNOWLEDGMENTS

We thank the anonymous reviewers for their helpful comments. The Hayabusa2 spacecraft was developed and built under the leadership of JAXA, with contributions from the German Aerospace Center (DLR) and the Centre National d'Études Spatiales (CNES) and in collaboration with NASA; Nagoya University; University of Tokyo; National Astronomical Observatory of Japan (NAOJ); University of Aizu; Kobe University; and other universities, institutes, and companies in Japan. We thank the many engineers, including N. Inaba at JAXA and T. Masuda, S. Yasuda, K. Matsushima, and T. Ohshima at NEC Corporation for their dedicated work on the Hayabusa2 mission. The STXM data were acquired at beam line 19A of the Photon Factory, High Energy Accelerator Research Organization, and at beam line 5.3.2.2 of the Advanced Light Source (ALS), Lawrence Berkeley National Laboratory. Use of the ALS was supported by the Department of Energy (contract no. DE-AC02-05CH11231). The synchrotron FTIR data were acquired at the SMS beamline of SOLEIL. The NanoSIMS facility at Muséum National d'Histoire Naturelle (MNHN) in Paris was established by funds from the CNRS, Région Ile de France, Ministère délégué à l'Enseignement supérieur et à la Recherche, and the Muséum National d'Histoire Naturelle. The FIB facility at the University of Tokyo is supported by the Advanced Characterization Nanotechnology Platform in the Nanotechnology Platform Project sponsored by the Ministry of Education, Culture, Sports, Science and Technology (MEXT), Japan. We thank N. Sugimura at Waseda University, Y. Fujioka at Tohoku University, and C. Sandt and F. Borondics at SOLEIL for technical support. We thank S. Kawakami at Gifu Shokoku University, T. Fagan at Waseda University, M. E. Zolensky at NASA Johnson Space Center, MNHN, and B. Fectay and C. Bidaud for providing the meteorite samples used in this study. **Funding:** H.Yab. was supported by KAKENHI from the Japan Society for the Promotion of Science (JSPS) (grant nos. JP20H05846, 19H01954, 18H04461, and 20H04615) and the Astrobiology Center Program of the National Institutes of Natural Sciences (NINS) (grant nos. AB312007, AB022001, and AB032004). Y.Taka., Y.Takeici., Y.K., H.Su., S.Y., and D.W. were supported by KAKENHI from JSPS (grant no. JP17H06458). H.Yab., Y.K., M.Has., and H.Su. were supported by the JSPS Core-to-Core program "International Network of Planetary Sciences." LBo. and E.Q. acknowledge funding from the Centre National d'Études Spatiales (CNES-France). L.R. acknowledges funding from the European Research Council through the consolidator grant HYDROMA (grant agreement no. 819587). C.E., J.D., E.D., and J.M. acknowledge funding from CNES (MIAM12), DIM-ACAV+ (C3E), LabEx P210, PCMI, and ANR (COMETOR ANR-18-CE31-0011). R.S. and B.D.G. acknowledge funding from NASA awards 80HQTR20T0014 and 80HQTR20T0050. L.N. acknowledges funding from NASA grants NNX16AK72G and 80NSSC20K0340. A.D., A.D.-B., and J.M. acknowledge funding from Paris Ile-de-France Region-DIM "Matériaux anciens et patrimoniaux." Centro de Química Estrutural (Z.M.) acknowledges the financial support of Fundação para a Ciência e Tecnologia (FCT) (grants UIDB/00100/2020, UIDP/00100/2020, and LA/P/0056/2020). **Author contributions:** H.Yab. led the research and wrote the paper with contributions from L.N., B.D.G., R.S., L.R., LBo., Y.K., and G.D.C. Sample preparation for the research: H.Yab., B.D.G., T.Oku., M.Has., C.E., LBo., M.Matsum., Y.E., K.Kam., and M.S.; Raman analyses: LBo., M.K., E.Q., G.M., and Y.K.; FTIR analyses: Y.K., E.Q., E.D., LBo., C.E., and J.D.; STXM analyses: B.D.G., H.Yab., Y.K., G.C., D.K., S.Sa.,

R.S., Y.Taka., T.Oh., H.Su., Y.Take., S.Y., D.W., and Y.Tam.; STEM-EELS-EDS analyses: R.S.; AFM-IR analyses: J.M., A.D., A.D.-B., E.D., C.E., J.D., and L.Be.; NanoSIMS analyses: L.R., L.N., M.V.-P., S.M., and J.Ba.; Interpretation and writing: H.Yab., L.N., R.S., B.D.G., R.L., L.B., Y.K., E.D., J.M., E.Q., M.K., G.D.C., C.E., S.Su., T.Oku., M.Has., and S.Tac.; Administration of the initial analysis: S.Tac., H.Yu., T.Na., T.No., R.O., H.Yab., H.Na., K.Sa., H.C.C., and D.S.L.; Sample curation: M.Ab., T.Oka., T.Yad., M.N., K.Yog., A.N., M.Yoshit., A.I., A.Miy., S.F., K.Hata., H.So., Y.H., K.Ku., T.U., T.H., D.Y., and R.F.; Sample collection at Ryugu: Y.Ts., T.S., F.T., S.Tan., M.O., R.T., H.Yan., H.Sa., M.Hay., T.I., S.H., Y.-i.I., A.F., Y.Takei., K.Yoshik., Y.M., G.O., H.T., N.O., S.K., K.S., Y.Ya., H.I., K.Ka., K.Yoshih., T.Yam., H.No., A.Miu., S.Su., K.Ki., Nao.H., R.H., T.Mo., E.T., T.O., N.Sa., N.N., K.M., R.N., K.W., H.Se., K.Ot., Y.Yo., Y.I., Y.S., M.Ya., C.H., T.Mi., M.Matsuo., Nar.H., M.Ar., C.O., M.I., H.Yan., S.Tac., R.O., S.W., T.Na., H.Yab., R.J., J.-P.B., M.G., S.Sc.,

K.Og., C.P., N.Sc., J.B., T.-M.H., and A.M.-S.; Project management: Y.Ts., S.W., M.Yoshik., M.F., and S.N. All authors discussed the results and commented on the manuscript. **Competing interests:** The authors declare that they have no competing interests. **Data and materials availability:** All images used in this study and machine-readable data files are available at the JAXA Data Archives and Transmission System (DARTS) at https://data.darts.isas.jaxa.jp/pub/hayabusa2/paper/sample/Yabuta_2022/. Data for all Hayabusa2 samples and other data from the mission are available at the DARTS archive at <https://www.darts.isas.jaxa.jp/curation/hayabusa2> and <https://www.darts.isas.jaxa.jp/planet/project/hayabusa2/>, respectively. The samples of Ryugu are curated by the JAXA Astromaterials Science Research Group; distribution for analysis is through an Announcement of Opportunity available at <https://jaxa-ryugu-sample-ao.net>. The samples we used are listed in table S1.

License information: Copyright © 2023 the authors, some rights reserved; exclusive licensee American Association for the Advancement of Science. No claim to original US government works. <https://www.science.org/about/science-licenses-journal-article-reuse>

SUPPLEMENTARY MATERIALS

[science.org/doi/10.1126/science.abn9057](https://doi.org/10.1126/science.abn9057)

Materials and Methods

Supplementary Text

Figs. S1 to S8

Tables S1 to S3

References (77–85)

Submitted 29 December 2021; accepted 21 December 2022
10.1126/science.abn9057